Aberrant laminin signaling drives melanocyte dedifferentiation and unveils a tractable therapeutic target in vitiligo

Fei Yang [1,2], Lingli Yang [1*], Sylvia Lai [1], Masafumi Yokota [1,2], Yasutaka Kuroda [1,2], Takuo Yuki [2], Yoshito Takahashi [2], Tetsuya Sayo [2], Takeshi Namiki [3], Hiroyuki Goto [4], Sho Hiroyasu [4], Shigetoshi Sano [5], Shintaro Inoue [6], Yoichi Mizukami [7], Daisuke Tsuruta [4], and Ichiro Katayama [1]

[1] Department of Pigmentation Research and Therapeutics, Graduate School of Medicine, Osaka Metropolitan University, Osaka, Japan
[2] Cosmetic Products Research, Research and Development, Kao Corporation, Odawara, Japan
[3] Department of Dermatology, Graduate School and Faculty of Medicine, Institute of Science Tokyo, Tokyo, Japan
[4] Department of Dermatology, Graduate School of Medicine, Osaka Metropolitan University, Osaka, Japan
[5] Department of Dermatology, Kochi Medical School, Kochi University, Kochi, Japan
[6] Department of Cosmetic Health Science, Gifu Pharmaceutical University, Gifu, Japan
[7] Institute of Gene Research, Yamaguchi University Science Research Center, Yamaguchi, Japan

[*] Correspondence to: L Yang, Department of Pigmentation Research and Therapeutics, Graduate School of Medicine, Osaka Metropolitan University, Osaka 5450051, Japan. E-mail: yang.lingli@omu.ac.jp.

Manuscript word:8148 Figure counts: 6 Supplementary figure counts: 16 **Supplementary table counts:** 8

Funding sources: This research was supported by JSPS KAKENHI Grant Numbers 22K08409 and 18K08267.

Conflicts of interest: The authors declare no conflicts of interest.

Ethics statement: The specimen collection and overall study design were approved by the Medical Ethics Committee of Osaka Metropolitan University (No. 4152).

Abstract

Vitiligo is an acquired depigmenting skin disorder characterized by progressive melanocyte loss, but the cellular mechanisms driving this process remain unclear. Here, we identify melanocyte dedifferentiation as a central and reversible pathogenic mechanism in vitiligo. In healthy human skin, melanocytes reside within a basement membrane niche defined by dystroglycan-laminin-211 adhesion. In contrast, vitiligo lesions exhibit aberrant extracellular matrix remodeling, leading to an adhesion switch to integrin α3β1-laminin-332 interactions. This shift promotes melanocyte dedifferentiation *via* Rho-F-actin-dependent activation of Hippo and MAPK pathways, resulting in c-Jun-mediated transcriptional changes. Dedifferentiated melanocytes lose their pigment-producing identity and acquire neural crest-like features with multilineage potential. Importantly, this process is reversible. Pharmacological inhibition of involved pathways restores melanocyte differentiation and induces repigmentation in both vitiligo mouse models and *ex vivo* patient skin. Notably, JAK inhibitors also promote redifferentiation independently of immune modulation. These findings uncover melanocyte dedifferentiation as a fundamental driver of vitiligo and a tractable therapeutic target, offering new opportunities for therapeutic intervention.

42 ## Introduction

43 Vitiligo is a common, acquired depigmenting disorder characterized by the progressive loss of functional
44 melanocytes from the epidermis[1]. Although extensive studies have implicated autoimmune responses in
45 disease initiation[2], the precise mechanisms underlying melanocyte disappearance remain incompletely
46 understood[3]. In addition to immune-mediated cytotoxicity, other factors, such as oxidative stress[4], defective
47 adhesion[5-7], metabolic dysregulation[8], and the accumulation of senescence-associated secretory phenotype
48 factors[9], have been proposed to contribute to melanocyte loss. However, whether melanocytes are entirely
49 eliminated or instead persist in a nonfunctional or dedifferentiated state remains a fundamental and
50 unresolved question with important clinical implications.

51 Melanocytes may persist in stable vitiligo lesions despite being morphologically altered, amelanotic, and
52 undetectable by conventional melanocyte markers such as tyrosinase (TYR), tyrosinase-related protein 1
53 (TYRP1), dopachrome tautomerase (DCT), premelanosome protein (PMEL), melanoma antigen recognized
54 by T-cells 1 (MART-1; also known as Melan-A), and melanocyte inducing transcription factor (MITF)[9-12].
55 These findings imply the existence of dedifferentiated or dormant melanocyte populations that evade
56 standard detection, raising the possibility that changes in the local skin microenvironment, particularly at the
57 basement membrane (BM), may play a critical role in regulating melanocyte identity and survival.

58 We previously reported structural abnormalities in the BM of vitiligo skin, including disorganized
59 laminin deposition[13]. This finding is consistent with earlier histopathological studies that identified
60 ultrastructural BM defects in vitiligo lesions[14-17], collectively pointing to BM disruption as a potentially
61 underappreciated factor in vitiligo pathogenesis[18-20]. Laminins, key components of the extracellular matrix
62 (ECM), are known to regulate cell adhesion, polarity, and fate in various tissue types[21-23]. Given the well-
63 established role of the ECM in defining tissue-specific niches and modulating cellular behavior, we

64 hypothesized that BM alterations may contribute to melanocyte dysfunction in vitiligo by disrupting cell-
65 matrix interactions.

66 Although the adhesion mechanisms of basal keratinocytes to the BM are well characterized, far less is
67 known about how melanocytes anchor to and interact with their surrounding matrix. Although several
68 adhesion molecules have been implicated in melanocyte-ECM binding[24-26], the specific laminin isoforms
69 involved, and their corresponding melanocyte receptors, remain poorly defined. Considering that laminins
70 exhibit isoform-specific and spatially restricted expression patterns[22,27], even subtle changes in BM
71 composition may profoundly affect melanocyte adhesion, stability, and phenotype.

72 To address this gap, we systematically investigated the composition of laminin isoforms surrounding
73 melanocytes in healthy and vitiligo skin and profiled their corresponding adhesion receptors. We found that
74 in healthy skin, melanocytes adhere to laminin-211 *via* dystroglycan, forming a previously unrecognized
75 adhesion architecture. In contrast, melanocytes in vitiligo lesions exhibited a striking adhesion switch to
76 laminin-332 engagement *via* integrin α3β1. Functional analyses revealed that this switch promotes
77 melanocyte dedifferentiation through Rho-F-actin-dependent activation of the Hippo and mitogen-activated
78 protein kinase (MAPK) signaling pathways, ultimately leading to c-Jun-driven transcriptional changes and
79 loss of pigment-producing identity.

80 Importantly, this dedifferentiated state was reversible. Pharmacological inhibition of key components in
81 this pathway restored melanocyte differentiation and stimulated repigmentation in both vitiligo mouse
82 models and patient-derived skin explants. These findings establish adhesion-dependent melanocyte
83 dedifferentiation as a key pathogenic mechanism in vitiligo and highlight the BM microenvironment as a
84 promising therapeutic target for restoring melanocyte function and skin pigmentation.

Results

Differential distribution of laminin isoforms in normal and vitiligo skin

First, we systematically examined the expression and distribution of laminin isoforms surrounding melanocytes in healthy and perilesional vitiligo skin. Immunofluorescence analysis revealed that in healthy skin, melanocytes were surrounded by laminin α2, β1, and γ1 (components of laminin-211), whereas laminin α3, β3, and γ2 (components of laminin-332) were selectively absent (Extended Data Fig. 1, Fig. 1a). In contrast, melanocytes in perilesional vitiligo skin exhibited prominent linear deposition of laminin α3, β3, and γ2, indicating a switch in the surrounding ECM composition (Fig. 1a). This observation was further supported by immuno-electron microscopy, which confirmed the absence of laminin α3 around melanocytes in healthy skin and its presence in vitiligo skin (Fig. 1b).

As integrins are currently known to serve as the main receptors for laminins[28], we next examined the expression of integrin isoforms in normal epidermal melanocytes and detected α2, α5, αv, β1, β3, and low levels of β4 (Extended Data Fig. 2). To detect laminin-integrin interactions *in situ*, we performed the proximity ligation assay (PLA), an antibody-based technology that enables the visualization of protein-protein interactions (Fig. 1c), on skin tissue sections from healthy controls (Extended Data Fig. 3, Fig. 1d). In keratinocytes, the PLA signal validated previously reported interactions[29], including integrin α6β4-laminin-332 (detected *via* integrin β4-laminin γ2), integrin α3β1-laminin-332 (detected *via* integrin β1-laminin γ2), and integrin α6β1-laminin-511 (detected *via* integrin β1-laminin α5) (Extended Data Fig. 3) . However, in melanocytes, although integrin β1, β3, and β4 subunits were expressed (Extended Data Fig. 2), no detectable interaction with laminin-211 (identified *via* laminin α2), the major isoform surrounding melanocytes in healthy skin, was observed (Extended Data Fig. 3). Nevertheless, a weak interaction between integrin β1 and laminin γ1 was detectable in melanocytes (Extended Data Fig. 3); this binding was substantially weaker than the integrin-laminin interactions observed between keratinocytes and the BM.

These findings suggest that in normal skin, melanocyte adhesion to the BM is unlikely to be primarily mediated by integrin-laminin-211 interactions.

Given prior reports that laminin-211 binds α-dystroglycan and integrin α7β1, particularly in muscle and neural tissues[27], we investigated whether dystroglycan contributes to melanocyte adhesion. Using PLA, we observed strong dystroglycan-laminin-211 binding in normal melanocytes, whereas this interaction was markedly diminished in vitiligo melanocytes (Fig. 1d). This finding indicates that in healthy skin, melanocyte adhesion to laminin-211 is primarily mediated by dystroglycan.

In the basal epidermis, normal melanocytes were positioned in distinct laminin-332- and laminin α5-deficient niches along the BM (Extended Data Fig. 1), while in vitiligo skin, melanocytes were closely associated with BM regions enriched in laminin-332 (Extended Data Fig. 1, Fig. 1a). Together with prior evidence implicating discoidin domain receptor family, member 1 (DDR1)-collagen IV interactions in melanocyte adhesion[25], we further examined these potential alternative adhesion pathways by PLA in healthy and perilesional vitiligo skin. In normal skin, melanocytes predominantly exhibited dystroglycan-laminin-211 binding, along with weak DDR1-collagen IV interactions. Notably, no laminin-332 or laminin α5 signals were detected at melanocyte-BM contact sites, resulting in melanocyte-specific gaps. In contrast, vitiligo melanocytes displayed robust integrin β1-laminin-332 binding, while other adhesion signals, including dystroglycan-laminin-211 and DDR1-collagen IV, were largely absent (Fig. 1d). These observations indicate that melanocyte adhesion mechanisms differ between healthy and vitiligo skin: normal melanocytes primarily rely on dystroglycan-laminin-211 interactions, whereas in vitiligo skin, adhesion is mediated predominantly through integrin β1-laminin-332 interactions (Fig. 1e).

To validate that dystroglycan-laminin-211 interaction is the predominant mechanism mediating melanocyte adhesion in healthy skin, we used antibody blockade, knockdown by small interfering RNA (siRNA), and enzymatic deglycosylation approaches. Blocking dystroglycan with specific antibodies

131 significantly impaired melanocyte adhesion to laminin-211-coated surfaces, whereas no significant effect
132 was seen with inhibition of integrin α7β1, the only other laminin-211 receptor identified to date aside from
133 dystroglycan[27]. Similarly, siRNA-mediated knockdown of dystroglycan or its glycosylation regulator
134 LARGE abolished adhesion to laminin-211. Enzymatic removal of glycosylation sites on dystroglycan also
135 reduced melanocyte-laminin-211 binding in a dose-dependent manner (Fig. 1f). These findings uncover a
136 clear molecular distinction between melanocyte adhesion mechanisms in healthy and vitiligo skin, reflecting
137 a pathological reorganization of the BM microenvironment.

138 **Laminin-332-mediated adhesion shift induces melanocyte dedifferentiation**

139 To investigate whether the altered adhesion environment observed in vitiligo skin affects melanocyte
140 behavior, we cultured primary human epidermal melanocytes on laminin-332 or laminin-211 and compared
141 their phenotypic and molecular characteristics. Interestingly, melanocytes on laminin-332 exhibited marked
142 morphological changes, becoming flattened with reduced dendricity, in contrast to the highly branched and
143 dendritic morphology observed on laminin-211 (Fig. 2a). Immunofluorescence analysis further revealed a
144 profound decrease in expression of melanogenic proteins, including PMEL17 and TYRP1, under laminin-
145 332 conditions (Fig. 2a).

146 To assess the effect of laminin-332 on melanocyte phenotype, we performed magnetic-activated cell
147 sorting (MACS) based on expression of c-Kit, a cell surface receptor that serves as a well-established marker
148 of the melanocytic lineage. Compared with melanocytes cultured on laminin-211, cells exposed to laminin-
149 332 exhibited a markedly increased c-Kit-negative population (Fig. 2b). Although c-Kit is not a definitive
150 marker of differentiation status, the loss of its expression may indicate a change in differentiation status,
151 suggesting that laminin-332 induces cellular reprogramming. Western blot analysis revealed markedly
152 reduced expression of key melanogenic proteins, including DCT, TYR, PMEL17, TYRP1, and Melan-A, in
153 both c-Kit-negative and c-Kit-positive subsets from laninin-332-treated cells compared with those cultured

154 on laminin-211 (Fig. 2c, d). Consistent with these molecular changes, melanin content was significantly
155 decreased in laminin-332-treated cultures (Fig. 2e, f). This phenotype was consistently observed across five
156 independent primary melanocyte lines (Extended Data Fig. 4), indicating that the response to laminin-332 is
157 reproducible and not limited to a specific cell line.

158 The dramatic changes in melanocyte morphology, marker expression, and pigment production prompted
159 us to investigate whether laminin-332 induces a dedifferentiated cell state. Transcriptomic profiling followed
160 by gene set enrichment analysis (GSEA) revealed significant upregulation of gene signatures associated with
161 embryonic stem cells and neural crest cells in laminin-332-treated melanocytes compared with those cultured
162 on laminin-211 (Fig. 2g), indicating the acquisition of a more plastic, progenitor-like state. To test the
163 functional significance of this reprogramming, we assessed the multilineage potential of laminin-332-treated
164 melanocytes in lineage-specific differentiation assays. Upon exposure to appropriate differentiation media,
165 these cells exhibited the capacity to transdifferentiate into neurofilament-positive neurons, collagen II-
166 producing chondrocytes, and alpha-smooth muscle actin-positive muscle-like cells (Fig. 2h), confirming
167 their dedifferentiated and multipotent phenotype. These results demonstrate that altered interactions with
168 laminin-332 induce a dedifferentiated melanocyte state, characterized by molecular and phenotypic changes
169 and reduced melanogenic capacity.

170 **Molecular and signaling mechanisms underlying laminin-332-induced melanocyte dedifferentiation**
171 **and modulation by external stimuli**

172 To investigate the molecular mechanisms underlying laminin-332-induced melanocyte dedifferentiation,
173 we performed bulk RNA sequencing of melanocytes cultured on laminin-332 or laminin-211. Laminin-332-
174 treated cells exhibited a distinct transcriptional profile, with a large number of differentially expressed genes
175 compared with laminin-211-treated controls (Fig. 3a). Melanogenic genes such as *MLANA*, *PMEL*, and *TYR*
176 were significantly downregulated, consistent with the observed reduction in pigment production (Fig. 2).

177 Conversely, several genes associated with the Hippo signaling pathway, including *TGFBI*, *CCN1*, *DKK1*,
178 *CCN2*, and *THBS1*, were markedly upregulated (Fig. 3a). Pathway enrichment analysis further revealed
179 significant activation of multiple signaling cascades, including the Hippo, PI3K (phosphatidylinositol 4,5-
180 bisphosphate 3-kinase catalytic subunit beta isoform)-Akt (protein kinase B), and MAPK pathways (Fig. 3b).
181 Enrichment of cytoskeleton-related pathways may also account for the cell flattening and morphological
182 changes observed in laminin-332-treated melanocytes (Fig. 2a).

183 To functionally validate the pathways implicated by transcriptomic analysis, we systematically silenced
184 key components of the Hippo, MAPK, and PI3K-Akt pathways in melanocytes cultured on laminin-332.
185 Small interfering RNA-mediated knockdown of Hippo pathway effectors (transcriptional coactivator YAP1;
186 transcriptional enhancer factor TEF-1 [also known as TEAD1]; CCN family member 1 [CCN1]; CCN family
187 member 2 [CCN2]) and MAPK components (serine/threonine-protein kinase B-raf [BRAF]; mitogen-
188 activated protein kinase 3 [MAPK3, also known as ERK1]; JNK1/MAPK8-associated membrane protein
189 [JNK1]) significantly increased the proportion of mature melanocytes, indicating suppression of
190 dedifferentiation (Fig. 3c, d). Similarly, knockdown of activator protein 1 (AP-1) transcription factors c-Jun
191 and c-Fos restored melanocyte differentiation (Fig. 3c, d). In contrast, knockdown of phosphatidylinositol
192 4,5-bisphosphate 3-kinase catalytic subunit alpha isoform (PIK3CA), glycogen synthase kinase-3 beta
193 (GSK3B), catenin beta-1 (CTNNB1), or neurogenic locus notch homolog protein 1 (NOTCH1) did not
194 significantly affect the dedifferentiated phenotype, suggesting that the PI3K-Akt pathway and other canonical
195 differentiation-related regulators do not play a major role in laminin-332-induced dedifferentiation.

196 Given that integrin signaling can activate both Hippo and MAPK cascades *via* Rho GTPase-mediated actin
197 remodeling[30,31], we tested whether direct cytoskeletal activation was sufficient to induce a dedifferentiation
198 phenotype comparable to that observed with laminin-332 treatment. Strikingly, treatment with a
199 Rho/Rac/Cdc42 activator, which promotes actin cytoskeleton reorganization, induced melanocyte

200 dedifferentiation even in the absence of laminin-332, closely resembling the phenotype observed under
201 laminin-332 treatment (Fig. 3e, f). These findings align with prior studies showing that both Hippo and
202 MAPK pathways can activate AP-1 transcriptional programs[32,33]. Western blot analysis further confirmed
203 that dedifferentiated melanocytes exhibited increased expression of cytoskeletal regulators (RhoA, Rac1/2/3,
204 Cdc42, F-actin), Hippo effectors (YAP, WW domain-containing transcription regulator protein 1 [TAZ],
205 CCN1, CCN2), MAPK signaling components (p-ERK, p-JNK), and AP-1 transcription factors, with c-Jun
206 showing the strongest induction (5.6-fold increase) (Extended Data Fig. 5a-d; quantified in Extended Data
207 Fig. 5e). These results demonstrate that c-Jun acts as a key downstream effector in laminin-332-induced
208 melanocyte dedifferentiation.

209 To further validate the role of c-Jun, we pharmacologically inhibited its upstream activator JNK using
210 SP600125, a selective JNK inhibitor. This intervention effectively blocked dedifferentiation induced by both
211 Rho/Rac/Cdc42 and YAP activation (Fig. 3e, f). In addition, inhibitors targeting the MAPK cascade revealed
212 that BRAF, MEK, and especially JNK inhibition suppressed dedifferentiation, whereas p38 inhibition had
213 no significant effect (Fig. 3g, h). These data are consistent with transcriptional network analyses showing
214 that JNK and ERK, but not p38, strongly regulate c-Jun expression and activity[34], highlighting c-Jun as the
215 key convergence point of the Rho-F-actin-Hippo-MAPK axis in melanocyte dedifferentiation.

216 We next investigated whether melanocyte dedifferentiation could be modulated by vitiligo-associated
217 extrinsic factors. Treatment of melanocytes with inflammatory cytokines (tumor necrosis factor alpha
218 [TNFα], interferon beta [IFNβ], interferon gamma [IFNγ], interleukin 1 beta [IL1β], interleukin 6 [IL6]) or
219 an oxidative stress inducer (hydrogen peroxide [H_2O_2]), all of which have been implicated in vitiligo
220 pathogenesis[35,36], induced dedifferentiation, as evidenced by loss of melanocyte markers (Extended Data Fig.
221 6a). However, the dedifferentiation response to these stimuli was less pronounced than that induced by
222 laminin-332 (Extended Data Fig. 6a), suggesting that diverse stress-related signals can trigger melanocyte

223 plasticity with varying efficiencies.

224 Interestingly, several JAK inhibitors, including ruxolitinib, delgocitinib, baricitinib, abrocitinib, and
225 tofacitinib, markedly suppressed laminin-332-induced melanocyte dedifferentiation (Extended Data Fig. 6b).
226 Given that these agents are typically used to suppress immune activation, our findings suggest an additional,
227 previously unrecognized mechanism by which JAK inhibition may directly promote melanocyte
228 differentiation, independent of immune modulation.

229 In light of our previous finding that the epidermal growth factor receptor (EGFR) inhibitor gefitinib
230 improved repigmentation in vitiligo animal models[37], we further tested whether other tyrosine kinase
231 inhibitors could affect melanocyte dedifferentiation. Inhibitors targeting EGFR, vascular endothelial growth
232 factor receptor 2, insulin-like growth factor 1 receptor (IGF1R), angiopoietin-1 receptor (Tie2), c-RET, and
233 ALK tyrosine kinase receptor (ALK) all attenuated laminin-332-induced dedifferentiation, with particularly
234 strong effects observed for EGFR, IGF-1R, c-RET, and ALK inhibitors (Extended Data Fig. 6c).

235 Numerous studies have previously linked tyrosine kinase signaling, reactive oxygen species, and
236 proinflammatory cytokines to the activation of MAPK and AP-1 pathways[33,38-40]. Collectively, our findings
237 demonstrate that melanocyte dedifferentiation is governed by an integrin-Rho-F-actin-Hippo/MAPK-c-Jun
238 signaling axis, and that this process is further modulated by extrinsic stimuli, including tyrosine kinase
239 signaling, oxidative stress, and cytokines (Extended Data Fig. 6d).

240 **Rho-F-actin-Hippo/MAPK-c-Jun signaling pathway regulates melanocyte differentiation across *in***
241 ***vitro*, *in vivo*, and *ex vivo* systems**

242 To confirm the functional relevance of the signaling pathways identified in Fig. 3, we examined the effects
243 of modulating Rho-F-actin, Hippo, and MAPK (JNK) signaling across three model systems: cultured primary
244 melanocytes (Fig. 4a), K14-Kitl transgenic mice (Fig. 4b), and *ex vivo* human skin explants (Fig. 4c).

245 In melanocyte cultures maintained on laminin-332, approximately 50% of cells retained a mature

246 phenotype, as indicated by Melan-A expression. Treatment with Rho/F-actin, YAP, or JNK inhibitors
247 markedly increased the proportion of Melan-A-positive melanocytes and markedly reduced the population
248 of dedifferentiated phalloidin-positive cells, effectively restoring a fully differentiated phenotype (Fig. 4a).
249 In contrast, treatment with activators of these pathways led to a pronounced reduction in mature melanocytes
250 and a corresponding increase in dedifferentiated cells. These findings support the conclusion that inhibition
251 of Rho-Hippo/MAPK signaling promotes melanocyte differentiation, while activation of these pathways
252 drives dedifferentiation, consistent with the mechanistic findings described above (Fig. 3).

253 We next assessed these effects *in vivo* using K14-Kitl transgenic mice, which exhibit melanocyte retention
254 in the dorsal epidermis. Two-week topical applications of Rho, YAP, or JNK inhibitors enhanced epidermal
255 pigmentation, as observed by bright-field microscopy (Fig. 4b). Immunofluorescence analysis revealed
256 increased numbers of mature melanocytes (TYRP1^{+}/c-Kit^{+}) in the basal epidermis. Conversely, 4-week
257 treatment with corresponding pathway activators led to hypopigmentation and decreased numbers of mature
258 melanocytes (TYRP1^{+}/c-Kit^{+}) in the basal epidermis, further confirming that these signaling pathways
259 regulate melanocyte differentiation status *in vivo.*

260 To evaluate the relevance of these findings in human tissue, we applied the same modulators to healthy
261 adult human skin explants. After 1 week of treatment, Rho, YAP, or JNK inhibition increased the number of
262 functional melanocytes, as evidenced by increased 3,4-dihydroxyphenylalanine (DOPA) staining and Melan-
263 A expression in the basal layer (Fig. 4c). In contrast, pathway activators reduced both DOPA^{+} and Melan-A^{+}
264 melanocyte populations.

265 Together, these results demonstrate that Rho-F-actin-Hippo/MAPK-c-Jun pathways act as central
266 regulators of melanocyte differentiation across multiple biological systems and ultimately determine
267 pigmentation outcomes in skin.

268 **Melanocyte dedifferentiation in patients with vitiligo**

269 Given our earlier observation that melanocytes in vitiligo skin are in direct contact with laminin-332 (Fig.
270 1), we next investigated whether the dedifferentiation mechanisms identified *in vitro* are also present in
271 patients' tissue. We first assessed melanogenic activity in perilesional skin using the DOPA reaction.
272 Compared with healthy controls, melanocytes in perilesional vitiligo skin showed markedly reduced DOPA
273 staining (Fig. 5a), demonstrating a reduction in pigment-producing capacity.

274 To identify reliable markers for dedifferentiated melanocytes in patient samples, we first compared
275 laminin-332-treated melanocytes with cultured melanoblasts. Both cell types lacked Melan-A expression,
276 but although melanoblasts typically retained early melanocytic markers such as c-Kit and DCT[41], laminin-
277 332-treated cells showed heterogeneous or absent expression of these markers, suggesting a dedifferentiation
278 state beyond the melanoblast stage. Notably, both melanoblast and laminin-332-induced dedifferentiated
279 cells exhibited strong expression of neural crest-associated markers SOX9 and tumor necrosis factor receptor
280 superfamily member 16 (NGFR), consistent with their developmental origin[42] (Extended Data Fig. 7).
281 Further immunophenotyping of laminin-332-treated melanocytes revealed a spectrum of differentiation
282 states: from fully differentiated cells (Melan-A^{+}/DCT^{+} or c-Kit^{+}, SOX9^{-}/NGFR^{-}) (Extended Data Fig. 8, cell
283 type #1), to intermediate dedifferentiating states (e.g., SOX9^{+} or NGFR^{+} with partial retention of Melan-A)
284 (Extended Data Fig. 8, cell type #2), to fully dedifferentiated cells lacking all melanocytic markers but
285 expressing SOX9 and/or NGFR (e.g., NGFR^{+}/SOX9^{+}) (Extended Data Fig. 8, cell type #3). These
286 observations provided a rationale for using SOX9 and NGFR as reliable markers for dedifferentiated
287 melanocytes in tissue analysis.

288 Although c-Kit and NGFR were undetectable in most perilesional melanocytes (Extended Data Fig. 9),
289 the combined assessment of DCT/SOX9 and Melan-A reliably identified dedifferentiating cells (Fig. 5b).
290 Specifically, dedifferentiated melanocytes were characterized either by a DCT-positive/Melan-A-negative

291 phenotype or by concurrent SOX9/Melan-A expression (Fig. 5b). These dedifferentiated cells often
292 expressed elevated F-actin and phosphorylated c-Jun (Fig. 5b), consistent with the cytoskeletal and
293 transcriptional changes observed under laminin-332–induced conditions *in vitro* (Fig. 3; Extended Data Fig.
294 5).

295 Previous studies have shown that SOX9 is expressed in melanoblasts and downregulated during
296 melanocyte differentiation[43]. SOX9 also antagonizes SOX10[44], a master regulator of melanocyte
297 differentiation *via* MITF activation[45], and plays a critical role in precursor fate determination in the hair
298 follicle niche[46]. Increased SOX9 expression has been reported in vitiligo melanocytes[47]. To test the functional
299 relevance of SOX9 in melanocyte dedifferentiation, we overexpressed SOX9 in cultured melanocytes using
300 an episomal pEBMulti vector. SOX9 overexpression, confirmed by His-tag colabeling, led to a marked
301 decrease in Melan-A expression (Fig. 5c), indicating loss of a mature melanocyte phenotype.

302 We next examined whether SOX9 is required for laminin-332–induced dedifferentiation. In melanocytes
303 cultured on laminin-332, siRNA-mediated knockdown of SOX9 (siSOX9) markedly suppressed the
304 dedifferentiation phenotype such that the proportion of Melan-A^{+} mature melanocytes significantly increased
305 compared with control (siMOCK)-transfected cells (Fig. 5d). These results demonstrate that SOX9 is
306 necessary for the dedifferentiation program triggered by laminin-332. As c-Jun has previously been shown
307 to transcriptionally activate SOX9[48], our findings suggest that SOX9 functions downstream of the Rho-F-
308 actin-Hippo/MAPK-c-Jun axis to drive phenotypic reprogramming of melanocytes in vitiligo.

309 Spatial transcriptome analysis of perilesional vitiliginous skin provided further molecular evidence for
310 melanocyte dedifferentiation. To classify melanocyte states, we first identified melanocyte-like cells based
311 on the presence of translucent cytoplasm on hematoxylin and eosin (H&E)-stained sections. Cells within this
312 morphological category were further classified as differentiated melanocytes (MCs) if they expressed
313 canonical melanogenic markers such as Melan-A or PMEL. In contrast, dedifferentiated or dedifferentiating

314 melanocytes (DeMCs) were defined as translucent H&E-positive cells that lacked Melan-A/PMEL
315 expression but showed positivity for DCT, SOX9, or NGFR.

316 Gene expression profiling revealed that DeMCs exhibited upregulation of genes associated with stemness
317 (e.g., *SOX9*, *NGFR*, *YY1*, *POU2F1*, *SOX4*, *LRIG1*), cytoskeletal remodeling (e.g., *RHOC*, *ACTB*, *RHOV*),
318 Hippo signaling components (e.g., *CCN5*, *CCN1*, *YAP1*), AP-1 family transcription factors (e.g., *JUN*, *JUNB*,
319 *ATF7*, *JUND*), and MAPK pathway kinases (e.g., *MAPK9*, *MAP3K13*, *MAP3K2*, *MAPK13*) (Fig. 5e). In
320 contrast, MCs predominantly expressed melanogenic genes such as *TYRP1*, *MLANA*, *TYR*, and *MITF* (Fig.
321 5e). The transcriptional signatures of DeMCs in patient skin closely mirrored those observed in laminin-332-
322 treated melanocytes *in vitro*, supporting the presence of a conserved dedifferentiation program.

323 **Pharmacological reversal of melanocyte dedifferentiation restores pigmentation across multiple**
324 **vitiligo models**

325 To explore the therapeutic potential of targeting melanocyte dedifferentiation, we tested the efficacy of
326 pharmacological inhibitors across multiple vitiligo model systems.

327 We first developed a three-dimensional (3D) human skin model with defined laminin-332 exposure,
328 allowing precise modulation of the melanocyte microenvironment. Laminin-332 coating induced a
329 concentration-dependent loss of pigmentation (Fig. 6a), generating sharply demarcated depigmented zones
330 (Fig. 6b) that recapitulate the lesion morphology observed in vitiligo. Immunostaining confirmed that
331 laminin-332 treatment decreased the number of Melan-A-positive mature melanocytes (Fig. 6c) while
332 increasing DCT-single-positive dedifferentiating melanocytes (Extended Data Fig. 10), consistent with a
333 dedifferentiation phenotype. Treatment with the JNK inhibitor SP600125 effectively reversed these changes,
334 restoring pigmentation and increasing the proportion of mature melanocytes (Fig. 6c).

335 To validate these findings *in vivo*, we used a rhododendrol-induced depigmentation model in K14-Kitl
336 mice[49]. Rhododendrol application resulted in progressive pigment loss in both fur and skin (Extended Data

337 Fig. 11a, b), with prominent melanocyte dedifferentiation at intermediate concentrations (10%) (Extended
338 Data Fig. 11c). In this rhododendrol-induced depigmentation model, both cytochalasin D (an actin
339 polymerization inhibitor) and SP600125 significantly restored pigmentation and increased TYRP1-positive
340 melanocytes in the epidermis (Fig. 6d), further supporting a central role for cytoskeletal and JNK signaling
341 in melanocyte dedifferentiation.

342 We next evaluated the therapeutic potential of dedifferentiation inhibition using *ex vivo* lesional skin
343 explants from patients with vitiligo. After 1 week of SP600125 treatment, DOPA staining revealed a marked
344 increase in DOPA-positive melanocytes compared with dimethyl sulfoxide (DMSO)-treated controls,
345 indicating restoration of melanogenic activity (Fig. 6f, top panels). Immunofluorescence analysis further
346 showed a significant increase in Melan-A-positive melanocytes in SP600125-treated samples, with these
347 cells localized along the BM as defined by collagen IV staining (Fig. 6f, bottom panels). In untreated explants,
348 many melanocytes were DCT-positive but lacked Melan-A expression, consistent with a dedifferentiated
349 phenotype. In contrast, SP600125 treatment induced re-expression of Melan-A in these DCT-positive cells
350 (Extended Data Fig. 12), supporting the reversal of the dedifferentiated state and restoration of a mature
351 melanocyte identity.

352 Together, these findings demonstrate that the inhibition of melanocyte dedifferentiation restores
353 pigmentation across 3D skin equivalents, mouse models, and patient-derived skin explants, supporting its
354 central role in vitiligo pathogenesis and suggesting that dedifferentiation reversal may represent a potential
355 therapeutic strategy for vitiligo (Fig. 6g).

356 ## Discussion

357 Following a "clinical-to-basic-to-clinical" research approach, this study identifies and elucidates the
358 molecular mechanism of melanocyte dedifferentiation in vitiligo and demonstrates its reversibility across
359 human tissue and disease models. In the present study, we uncovered a previously unrecognized mechanism
360 contributing to melanocyte loss in vitiligo. Rather than a complete disappearance of melanocytes, cells in
361 lesional skin exhibit a dedifferentiated phenotype. In healthy human skin, melanocytes are located within
362 specialized BM niches characterized by the presence of laminin-211 and the absence of laminin-332. In
363 contrast, vitiligo skin displays pathological BM remodeling, with aberrant accumulation of laminin-332
364 around melanocytes. This shift in laminin composition disrupts cell-matrix interactions and triggers
365 intracellular signaling cascades. Through systematic pathway analysis, we demonstrate that laminin-332
366 binding to integrin β1 initiates Rho-dependent cytoskeletal remodeling, leading to activation of the Hippo
367 and MAPK pathways, ultimately resulting in c-Jun activation. Functionally, this signaling suppresses
368 melanocyte differentiation markers, reduces melanin synthesis, and induces a transcriptional program
369 associated with neural crest-like progenitor cells. Notably, this dedifferentiation process is reversible.
370 Pharmacological inhibition of key signaling restored pigmentation and melanogenic marker expression in
371 3D skin equivalents, a rhododendrol-induced leukoderma mouse model, and *ex vivo* patient-derived skin
372 explants.

373 To understand how this laminin-332-deficient niche is maintained in healthy skin and disrupted in
374 vitiligo, we investigated the role of melanocyte-derived matrix-degrading enzymes. In normal human skin,
375 melanocytes expressed high levels of the membrane-type matrix metalloproteinases MT1-MMP (MMP14)
376 and MT4-MMP (MMP17), as confirmed by immunostaining and validated in multiple skin-derived cell lines
377 (Extended Data Fig. 13a-d). Functional assays further demonstrated that melanocytes actively degrade
378 laminin-332, forming clear pericellular clearance zones; this activity was significantly impaired upon

379 knockdown of either MT1-MMP or MT4-MMP (Extended Data Fig. 13e). In vitiligo, epidermal melanocytes
380 exhibited reduced MT4-MMP expression, accompanied by abnormal accumulation of laminin-332
381 (Extended Data Fig. 14a-b). These findings are consistent with our previous observations of aberrant laminin-
382 332 distribution and BM disorganization in vitiligo skin[13]. Although the mechanisms underlying MT4-MMP
383 downregulation remain to be clarified, decreased expression or functional abnormalities of MT4-MMP in
384 melanocytes diminished their ability to degrade laminin-332, thereby destabilizing this specialized niche.
385 Moreover, other laminin-332-degrading enzymes[50], including MMP2, MMP9, MMP3, neutrophil elastase,
386 cathepsin G, plasmin, and others, may release laminin-332 fragments that accumulate around melanocytes
387 and further disrupt niche integrity. In vitiligo, we previously observed an enrichment of MMP2 near the BM[13].
388 These concurrent alterations may accelerate the damage to the laminin-332-deficient niche, ultimately
389 promoting melanocyte dedifferentiation in vitiligo. Additionally, mouse melanocytes lacked expression of
390 both MT1-MMP and MT4-MMP (Extended Data Fig. 14c), limiting the translational utility of mouse models
391 for studying melanocyte-matrix interactions and ECM remodeling in human skin.

392 In addition to ECM remodeling, alterations in melanocyte adhesion receptors contribute to niche
393 instability. In healthy skin, melanocytes primarily adhere to the BM *via* dystroglycan-laminin-211
394 interactions (Fig. 1d). In vitiligo, this adhesion is markedly reduced (Fig. 1d), likely due to decreased
395 dystroglycan expression in perilesional melanocytes (Extended Data Fig. 15a). Given that dystroglycan is a
396 known substrate of MMP2[51], and our previous studies have shown elevated MMP2 levels in patients with
397 vitiligo[13], this reduction may be attributed to enhanced proteolytic degradation by MMP2. We also found that
398 exposure to laminin-332 downregulates dystroglycan expression in melanocytes (Extended Data Fig. 15b),
399 suggesting a potential feedback loop. Reduced dystroglycan weakens laminin-211 binding, facilitating
400 compensatory engagement with laminin-332, which further promotes dedifferentiation and suppresses
401 dystroglycan expression. These findings establish dystroglycan as a critical adhesion receptor for

402 melanocytes. Interestingly, dystroglycan defects also lead to melanocyte detachment in congenital muscular
403 dystrophy (CMD)[52], although patients with CMD do not display vitiligo-like depigmentation, possibly due
404 to the absence of dedifferentiation-inducing cues such as laminin-332 accumulation. Given dystroglycan's
405 conserved roles in muscle and nervous systems[53], and the shared neural crest origin of melanocytes[54], our
406 findings suggest that melanocytes may serve as a useful model for investigating CMD-associated
407 neurodevelopmental abnormalities.

408 The dedifferentiation phenotype described here has important implications for vitiligo pathogenesis.
409 Flattened melanocytes observed in vitiliginous skin and culture have been previously noted[55-57], and some
410 have been shown to regain function upon oxidative stress relief[10]. Our findings provide molecular evidence
411 that melanocytes in lesional vitiligo skin are not completely absent, but rather persist in a dedifferentiated,
412 nonpigmented state. Although we identified candidate markers, including c-Kit, DCT, NGFR, and SOX9,
413 the heterogeneity in their expression, along with the presence of fully dedifferentiated, marker-negative cells,
414 suggests that additional work is needed to define robust and universal markers for detecting dedifferentiated
415 melanocytes in human tissue. This concept of reversible melanocyte dedifferentiation is further supported by
416 recent work in hair follicle biology. A 2023 study by Sun et al.[50] demonstrated that melanocyte stem cells
417 within the hair follicle niche dynamically transition between stem- and transit-amplifying states through
418 reversible dedifferentiation in response to local cues such as WNT signaling. These findings align with our
419 observations in vitiligo, suggesting that melanocyte fate plasticity, whether in hair follicles or the
420 interfollicular epidermis, may be broadly governed by niche-dependent and reversible dedifferentiation
421 programs.

422 Mechanistically, we showed that melanocyte dedifferentiation was mediated by the integrin α3β1-Rho-F-
423 actin-Hippo/MAPK-c-Jun signaling upon laminin-332 binding. Notably, JNK inhibition with SP600125
424 reversed this process, restoring melanocyte morphology and pigmentation. Although inhibitors targeting Rho,

425 YAP, and JNK were effective in our models, their current clinical applications are limited to oncology,
426 indicating the need for further development of melanocyte-targeted compounds suitable for vitiligo treatment.
427 Interestingly, JAK inhibitors enhanced melanocyte differentiation independent of their immunomodulatory
428 effects, possibly *via* STAT3-mediated regulation of AP-1 components c-Jun/c-Fos[58]. This mechanism further
429 supports the clinical application of JAK inhibitors, although more targeted agents may offer promising
430 efficacy and safety in the future.

431 Cellular differentiation and dedifferentiation are fundamental processes in development, regeneration, and
432 disease. Although dedifferentiation has been extensively studied in cultured cells, particularly in induced
433 pluripotent stem cells[59], it occurs rarely in adult human tissues and typically under severe stress or injury[60,61].
434 Our findings establish melanocytes as a model for stress-induced dedifferentiation in skin. In studies of ocular
435 lineage differentiation from induced pluripotent stem cells, laminin-211 has been shown to direct
436 differentiation toward the neural crest lineage, whereas laminin-332 directs differentiation toward the
437 epithelial lineage[62]. This finding aligns with our observation that laminin-211 supports melanocyte
438 differentiation, whereas laminin-332 promotes dedifferentiation (Fig. 2). Furthermore, mice engineered to
439 express laminin-211 in the BM show a human-like melanocyte localization in the basal layer[63], indicating
440 laminin-211's essential role in niche structure and melanocyte retention.

441 Taken together, our study demonstrates that the pathological microenvironment in vitiligo could trigger
442 melanocyte dedifferentiation through Rho-F-actin-dependent activation of Hippo and MAPK pathways,
443 ultimately leading to c-Jun activation (Fig. 3 and Extended Data Fig. 16). Consistent with previous reports,
444 Hippo signaling is known to regulate epithelial tissue reprogramming[64] and cooperate with paired box protein
445 Pax-3to modulate MITF expression in neural crest cells, thereby influencing melanocyte fate specification[65].
446 In addition to the core pathway identified, our data suggests that other microenvironmental factors, including
447 reactive oxygen species, proinflammatory cytokines, and other tyrosine kinase inhibitors, also contribute to

448 melanocyte differentiation (Extended Data Fig. 6). Although individual cytokines and tyrosine kinase
449 inhibitors exert modest effects, their combined influence *in vivo* may be substantially amplified. These
450 findings indicate the importance of targeting both intrinsic signaling and extrinsic niche components in
451 therapeutic strategies. The identification of melanocyte dedifferentiation as a reversible process not only
452 offers new therapeutic opportunities for vitiligo (Fig. 6) but also raises the possibility of modulating skin
453 pigmentation under physiological conditions (Fig. 4), with potential applications in cosmetic dermatology
454 and pigmentation disorders. This work represents a significant advance in understanding vitiligo
455 pathogenesis and highlights promising new therapeutic strategies. Future research should focus on
456 identifying more specific markers for dedifferentiated melanocytes and on developing safe, selective targeted
457 therapies.

458 # Methods

459 ## Human skin specimens

460 Frozen biopsies were obtained from lesional and perilesional skin of well-defined patients with
461 nonsegmental vitiligo (n = 15, ten patients in a progressive state and five patients in a stable state)
462 (Supplementary Table 1) and from corresponding sites on healthy donors (n = 7). The progressive state of
463 vitiligo was defined by the development of new lesions or the extension of pre-existing lesions in the previous
464 6 months, and the stable state was defined by no increase in the size of existing lesions and an absence of
465 new lesions in the previous year. Written informed consent was obtained from all participants prior to study
466 inclusion. The study was approved by the Medical Ethics Committee of Osaka Metropolitan University (No.
467 4152). All procedures involving human subjects were in accordance with the Helsinki Declaration of 1975,
468 as revised in 1983.

469 ## Cell culture

470 Primary human melanocytes, including HEMn-DP (#C2025C, Thermo Fisher Scientific, Waltham, MA,
471 USA), HEMn-MP (#C1025C, Thermo Fisher Scientific), and other human epidermal melanocytes (#LMC,
472 #LC1C1022, and #M4C0760) obtained from Kurabo Co. (Osaka, Japan), were cultured in medium 254
473 (Cascade Biologics, Invitrogen, Waltham, MA,, USA). Melanoblasts (36011-12, Celprogen, Torrance, CA,
474 USA) were maintained in Human Melanoblast Stem Cell Serum Free Media (#M36011-12, Celprogen) using
475 precoated flasks (#E36011-12-T75, Celprogen). All cell lines were incubated at 37 °C in a humidified
476 atmosphere containing 5% CO_2. For laminin-coating experiments, culture plates were treated overnight at
477 4 °C with either 20 μg/mL laminin-211 (#LN211-02, BioLamina, Sundbyberg, Sweden) or 20 μg/mL
478 laminin-332 (#LN332-02, BioLamina).

479 **Antibody neutralization experiments**

480 Melanocytes were preincubated with one of the following antibodies at a final concentration of 10 μg/mL
481 for 30 minutes: rabbit IgG control (#ab172730, Abcam, Cambridge, UK), mouse IgG control (#ab37355,
482 Abcam), anti-dystroglycan (#ab234587, Abcam), anti-integrin β1 (#PA5-29606, Thermo Fisher Scientific),
483 and anti-integrin α7 (#ab195959, Abcam). After pretreatment, cells were seeded onto laminin-211–coated
484 coverglass (#C018001, Matsunami Glass Ind., Ltd., Osaka, Japan) and incubated for 4–6 hours before
485 evaluating cell adhesion.

486 **Melanin content measurement**

487 Harvested cells were solubilized in Solvable solution (6NE9100, Perkin Elmer, Waltham, MA, USA) at
488 80 °C for 30 minutes. The melanin content of each sample was then quantified by measuring its absorbance
489 at 405 nm using a spectrophotometer. A standard curve generated with a synthetic melanin standard (M8631,
490 Sigma-Aldrich, St. Louis, MO, USA) was used to calculate the melanin concentration in each sample.

491 **Multilineage differentiation**

492 To assess differentiation potential, laminin-332–treated, dedifferentiated melanocytes were cultured in
493 lineage-specific induction media. For neural differentiation, cells were maintained in Mesenchymal Stem
494 Cell Neurogenic Differentiation Medium (#C-28015, PromoCell, Heidelberg, Germany). For chondrogenic
495 differentiation, the MesenCult-ACF Chondrogenic Differentiation Medium (#ST-05455, Veritas, Tokyo,
496 Japan) was used. For mesodermal differentiation, cells were cultured in a 1:1 mixture of Dulbecco's Modified
497 Eagle's Medium (DMEM; #D5921, Sigma-Aldrich) and F-12 (#N4888, Sigma-Aldrich), supplemented with
498 1× nonessential amino acid solution (#139-15651, FUJIFILM Wako Pure Chemical Corporation, Osaka,
499 Japan), 60 pM recombinant human TGF-beta 1 protein (#240-B-010/CF, R&D Systems, Minneapolis, MN,
500 USA), 10% fetal calf serum (#10270106, Thermo Fisher Scientific), and 1× penicillin-streptomycin solution

501 (#168-23191, FUJIFILM Wako Pure Chemical Corporation). Differentiation was evaluated after 1–4 weeks
502 using appropriate lineage-specific markers.

503 **MACS cell sorting**

504 c-Kit-positive and c-Kit-negative cell populations were isolated using MACS. Sorting was performed
505 using a MiniMACS Starting Kit (#130-090-312, Miltenyi Biotec, Bergisch Gladbach, Germany) and a
506 CD117 MicroBead Kit (#130-091-332, Miltenyi Biotec), following the manufacturer's instructions.

507 **3D skin model**

508 Three-dimensional skin models containing a dermal compartment were constructed in accordance with
509 our previously established protocol[13]. Briefly, human dermal fibroblasts were embedded in an acidic collagen
510 solution (KKN-IAC-50, Koken Co. Ltd, Tokyo, Japan). Following a 48-hour gel contraction period,
511 melanocytes or melanoblasts were coseeded with keratinocytes onto the contracted dermal equivalent. For
512 spatially controlled laminin-332 treatment, specific regions were defined using culture inserts (#80209, ibidi
513 GmbH, Gräfelfing, Germany). After laminin-332 coating and removal of the culture inserts, melanocytes
514 and keratinocytes were coseeded to form the epidermal layer. These 3D skin models were subsequently
515 maintained at the air-liquid interface for 10 days.

516 **Mouse experiments**

517 Eight-week-old male K14-Kitl mice (#RBRC00694, RIKEN BioResource Research Center, Tsukuba,
518 Japan) were used for all *in vivo* experiments. Rhododendrol (4-(4-hydroxyphenyl)-2-butanol) was generously
519 provided by Kanebo Cosmetics Inc. (Tokyo, Japan). A stock solution of 20% (w/v) rhododendrol was
520 prepared in a 50:50 (v/v) ethanol/sesame oil mixture as the vehicle. To establish a leukoderma mouse model,
521 mice were treated topically with 100 μL of 20% (w/v) rhododendrol on the dorsal skin once daily for 1 month.

522 This induction period was followed by a 2-week drug intervention phase. To specifically examine
523 melanocyte dedifferentiation, additional mice received a single topical application of rhododendrol 24 hours
524 before tissue collection and analysis. Specifically, 100 μL of a 5%, 10%, or 15% (w/v) rhododendrol solution
525 was applied to the dorsal skin of each mouse. All animal experiments were conducted in accordance with
526 protocols approved by the Institutional Animal Care and Use Committee (Approval No. 23018).

527 **Immunofluorescence and immunohistochemistry**

528 Frozen skin sections (6-μm thick) were fixed in 4% paraformaldehyde (163-20145, FUJIFILM Wako Pure
529 Chemical Corporation) for 15 minutes at room temperature, followed by blocking with 5% bovine serum
530 albumin for 30 minutes. Sections were then incubated with primary antibodies (Supplementary Table 2),
531 diluted 1:100 in blocking solution, overnight at 4 °C. Following primary antibody incubation, sections were
532 washed three times for 5 minutes each with phosphate-buffered saline (PBS) containing 0.05% Tween 20
533 (161-24801, FUJIFILM Wako Pure Chemical Corporation). Appropriate secondary antibodies
534 (Supplementary Table 3), diluted 1:1000 in blocking solution, were then applied for 1 hour at room
535 temperature in the dark. Sections were subsequently washed three times with 0.05% Tween 20 in PBS for 5
536 minutes per wash. Nuclei were counterstained with 4′,6-diamidino-2-phenylindole (DAPI; 340-07971,
537 FUJIFILM Wako Pure Chemical Corporation). Slides were imaged using an LSM 710 confocal laser
538 scanning microscope (ZEISS Group, Oberkochen, Germany), and images were acquired with ZEN 2012
539 software (ZEISS Group). Quantification of positively stained cells and mean fluorescence intensity was
540 performed using ImageJ software (National Institutes of Health, https://imagej.net/ij/index.html).

541 **Immuno-electron microscopy**

542 Skin tissues were fixed in 4% paraformaldehyde (163-20145, FUJIFILM Wako Pure Chemical
543 Corporation) for 30 minutes at room temperature, and then washed three times in PBS (5 minutes each).

544 Tissues were then cryoprotected by immersion in 30% sucrose at 4 °C overnight and subsequently embedded
545 in OCT compound (#45833, Funakoshi Co., Ltd., Tokyo, Japan). Frozen sections (7 μm thick) were prepared
546 and permeabilized in 0.25% saponin (#47036, MilliporeSigma, Burlington, MA, USA) for 30 minutes.
547 Sections were blocked for 30 minutes in PBS containing 0.1% saponin, 10% bovine serum albumin (#014-
548 15151, FUJIFILM Wako Pure Chemical Corporation), 10% normal goat serum (#16210072, Thermo Fisher
549 Scientific), and 0.1% gelatin from cold water fish skin (#G7041, MilliporeSigma). Samples were then
550 incubated with the primary antibody against laminin α3 (#FDV-0024, Funakoshi) diluted in blocking buffer
551 overnight at 4 °C. Following several washes, the sections were incubated with nanogold-conjugated anti-
552 mouse IgG (1.4 nm in diameter; 1:200; #2001, Nanoprobes, Yaphank, NY, USA) in blocking solution for 2
553 hours at room temperature. The nanogold signal was enhanced using the GoldEnhance EM kit (#2113,
554 Nanoprobes) for 4 minutes at room temperature. Samples were postfixed in 1% osmium tetroxide (#157-
555 01141, FUJIFILM Wako Pure Chemical Corporation), dehydrated through a graded ethanol series, and
556 embedded in TAAB EPON 812 embedding resin (#342-2, Nisshin EM, Tokyo, Japan). Ultrathin sections
557 (70 nm) were cut, stained with uranyl acetate and lead citrate, and imaged using a Talos F200C G2
558 transmission electron microscope (Thermo Fisher Scientific) equipped with a CCD-based camera system
559 (Advanced Microscopy Techniques, Woburn, MA, USA).

560 **Proximity ligation assay**

561 Frozen human skin sections were blocked with Duolink blocking solution (#DUO82007, MilliporeSigma)
562 for 30 minutes at 37 °C. The sections were then incubated overnight at 4 °C with primary antibodies (diluted
563 1:100). After this incubation, the sections were washed in Duolink *In Situ* Wash Buffer A (#DUO82046,
564 MilliporeSigma) and subsequently incubated with Duolink *In Situ* PLA Probes (Anti-Mouse PLUS,
565 #DUO92001; Anti-Rabbit MINUS, #DUO92005; MilliporeSigma) for 90 minutes at 37 °C. This step was
566 followed by ligation and signal amplification using the Duolink *In Situ* Detection Reagents Red kit

567 (#DUO92008, MilliporeSigma). For costaining of melanocytes, an anti-c-Kit antibody (#AF332, R&D
568 Systems) was included along with the other primary antibodies during the overnight incubation. During the
569 PLA probe incubation step, a corresponding Alexa Fluor Plus 488–conjugated donkey anti-goat IgG
570 (#A32814, Thermo Fisher Scientific) was added to detect the c-Kit primary antibody. This approach allowed
571 the simultaneous visualization of melanocytes in the tissue sections during the PLA probe incubation step.
572 After a final wash in Duolink *In Situ* Wash Buffer B (#DUO82048, MilliporeSigma) for 30 minutes, the
573 sections were mounted with Duolink *In Situ* Mounting Medium containing DAPI (#DUO82040,
574 MilliporeSigma) to counterstain nuclei. The slides were then examined under an LSM 710 confocal laser
575 scanning microscope (ZEISS Group), and fluorescent images were captured using ZEN 2012 software
576 (ZEISS Group).

577 **RNA sequencing and analysis**

578 RNA sequencing and library preparation were performed by Takara Bio Inc. (Shiga, Japan) using the
579 SMART-Seq v4 Ultra Low Input RNA protocol. Sequencing was conducted on a NovaSeq 6000 platform
580 with NovaSeq Control Software v1.7.5, Real Time Analysis v3.4.4, bcl2fastq2 v2.20, and DRAGEN Bio-IT
581 Platform v3.9.3 (Illumina, San Diego, CA, USA). Each experimental group included three biological
582 replicates, with a mean sequencing depth of approximately 55.08 million reads per sample. Reads were
583 aligned to the human genome (GRCh38.primary_assembly.genome.fa.gz) using GENCODE annotation (v39;
584 gencode.v39.primary_assembly.annotation.gtf.gz). Differential gene expression analysis was conducted
585 using DESeq2, and gene ontology enrichment analysis was performed with SRplot[66]. Gene set enrichment
586 analysis (GSEA) was carried out using GSEA v4.3.3 in accordance with the official GSEA User Guide, with
587 gene sets derived from the c2.cp.wikipathways.v2024.1.Hs.symbols collection.

588 **Spatial transcriptomics**

589 Spatial transcriptomic analysis was performed using the Visium HD Spatial Gene Expression platform
590 (10x Genomics, Pleasanton, CA, USA) at the Yamaguchi University Institute of Gene Research. A formalin-
591 fixed, paraffin-embedded (FFPE) skin tissue block from a perilesional area of patients with nonsegmental
592 vitiligo was analyzed. From each FFPE block, two consecutive 5-μm sections were cut and directly mounted
593 onto Visium HD capture slides. RNA was extracted from adjacent sections to assess integrity and purity;
594 only samples meeting internal quality thresholds for degradation proceeded to library preparation. After
595 placement, the tissue sections underwent H&E staining. A 6.5-mm × 6.5-mm capture area containing 2-μm
596 high-density spots was used to spatially profile approximately 18,000 genes at near single-cell resolution.
597 Downstream data processing, including quality control, gene expression mapping, and clustering analysis,
598 was performed using Loupe Browser (10x Genomics), enabling spatially resolved transcriptomic profiling
599 of the vitiligo skin tissue.

600 **Western blot analysis**

601 Protein extraction from cell pellets and the subsequent Western blot analysis were performed as described
602 in our previous study[67]. In each assay, 5 μg of extracted protein was used. Primary antibodies were applied
603 at the dilutions specified in Supplementary Table 4, with the anti-glyceraldehyde 3-phosphate dehydrogenase
604 antibody serving as the internal loading control. Signal intensities of the immunoreactive bands were
605 quantified using ImageJ densitometry software (National Institutes of Health,
606 https://imagej.net/ij/index.html).

607 **DOPA reaction**

608 Frozen skin sections were fixed in 1% glutaraldehyde for 1 hour and then washed 2 to 3 times with PBS.
609 The sections were then incubated at 37 °C for 2 hours in a 0.1% L-DOPA solution (#043-30563, FUJIFILM

610 Wako Pure Chemical Corporation) to facilitate melanin synthesis, as L-DOPA serves as a substrate for
611 tyrosinase activity. After incubation, the sections were washed 2 to 3 times with PBS and postfixed with
612 glutaraldehyde (#071-02031, FUJIFILM Wako Pure Chemical Corporation). Subsequently, the sections were
613 washed, dehydrated through an ethanol series, and mounted for microscopic observation.

614 **siRNA knockdown**

615 Human epidermal melanocytes were transfected with siRNAs using Lipofectamine RNAiMAX
616 transfection reagent (#13778030, Thermo Fisher Scientific) in accordance with the manufacturer's
617 instructions. Each siRNA was used at a final concentration of 30 nM. Six hours after transfection, the medium
618 was replaced with fresh growth medium. Knockdown efficiency for each target gene was confirmed by
619 quantitative real-time polymerase chain reaction (qPCR) on extracted RNA. A nontargeting siRNA
620 (siMOCK; #AM4611, Thermo Fisher Scientific) was used as a negative control. Target-specific siRNAs
621 (Thermo Fisher Scientific Silencer Select siRNAs) were used to knock down the genes listed in
622 Supplementary Table 5. All siRNA reagents were purchased from Thermo Fisher Scientific.

623 **Glycosidase digestion and cell adhesion assay**

624 Melanocytes were seeded on laminin-211–coated coverglass (#C018001, Matsunami Glass Ind., Ltd.).
625 Glycosidase digestion was performed in Opti-MEM medium (#31985070, Thermo Fisher Scientific) at 37 °C.
626 To remove O-linked oligosaccharides from α-dystroglycan on the cell surface, cells were first incubated with
627 neuraminidase (0.1-0.5 U/mL; #P0720S, New England Biolabs, Ipswich, MA, USA) for 2 hours. This
628 neuraminidase treatment cleaved terminal sialic acid residues, thereby exposing the underlying O-linked
629 oligosaccharide chains on α-dystroglycan. After the 2-hour incubation, the neuraminidase-containing
630 solution was aspirated, and cells were gently washed with PBS. Subsequently, cells were incubated with O-
631 glycosidase (0.05-0.5 U/mL; #P0733S, New England Biolabs) in fresh Opti-MEM medium for another 2

632 hours to remove the exposed oligosaccharides. Controls were treated with Opti-MEM-containing enzyme
633 buffer alone under identical conditions. Cell adhesion to laminin-211-coated coverslips was evaluated by
634 microscopy 2 to 6 hours post-treatment.

635 **Overexpression of SOX9 in human epidermal melanocytes**

636 Human epidermal melanocytes were transfected with either a human SOX9–expressing episomal plasmid
637 or an empty vector control. The SOX9 expression vector was a customized pEBMulti-Puro episomal plasmid
638 (FUJIFILM Wako Pure Chemical Corporation) carrying the human *SOX9* gene. Transfections were
639 performed using the Neon NxT Electroporation System (#N1096, Thermo Fisher Scientific) in accordance
640 with the manufacturer's instructions. Each transfection reaction contained 2 μg of episomal vector DNA
641 mixed with Lipofectamine LTX transfection reagent (#15338030, Thermo Fisher Scientific). At 24, 48, and
642 72 hours post-transfection, cells were fixed for immunofluorescence analysis to assess SOX9 overexpression.
643 Fixed cells were incubated with primary rabbit antibodies against SOX9 (rabbit anti-SOX9, #AB5535,
644 Sigma-Aldrich), Melan-A (mouse IgG2b anti-Melan-A, #917902, BioLegend, San Diego, CA, USA), and
645 the His-tag (rabbit IgG1 anti-His-tag, #12698, Cell Signaling Technology, Danvers, MA, USA). The stained
646 samples were then examined by fluorescence microscopy. The presence of robust nuclear SOX9
647 immunoreactivity and positive His-tag staining indicated successful overexpression of the *SOX9* transgene
648 in the transfected melanocytes.

649 ***Ex vivo* culture of human skin explants**

650 Full-thickness human skin explants were obtained from healthy donors and patients with vitiligo after
651 obtaining informed consent. For experiments involving healthy skin (Fig. 4), tissues were collected from
652 three independent donors. Each donor's tissue was divided into multiple small explants, and each drug-
653 treatment condition was assessed with three biological replicates (n = 3 per condition). For vitiligo skin (Fig.

654 6), a total of four 4-mm punch biopsies (two biopsies per patient) were obtained from the edge of lesional
655 areas from two patients. Each biopsy was bisected, generating paired control and drug-treated samples,
656 resulting in four biological replicates for each treatment condition (n = 2 per condition). Explants from
657 healthy donors and patients with vitiligo were cultured and analyzed separately. Each skin explant was placed
658 on a cell culture insert (8-µm pore size, #141082, Thermo Fisher Scientific) with the dermal side in contact
659 with the culture medium and the epidermal side exposed to air. The culture medium consisted of DMEM
660 (#044-29765, FUJIFILM Wako Pure Chemical Corporation) supplemented with 10% fetal bovine serum
661 (#10270106, Thermo Fisher Scientific) and 1× penicillin-streptomycin solution (#168-23191, FUJIFILM
662 Wako Pure Chemical Corporation). Explants were maintained at 37 °C in a humidified 5% CO_2 incubator
663 for 7 days, a duration well within the viability window reported for *ex vivo* human skin cultures. The culture
664 medium was refreshed every 2 days. Drug treatments were administered by adding test compounds directly
665 to the culture medium. Treatments were applied at the time of medium change to ensure consistent exposure,
666 and the vehicle control consisted of an equivalent volume of DMSO in the medium.

667 **Drug treatment methods**

668 For *in vitro* experiments, cells were cultured in Medium 254 (#M254500, Thermo Fisher Scientific)and
669 treated for 24 to 48 hours with various compounds dissolved in DMSO. Control cells received an equivalent
670 volume of DMSO as a vehicle control. Prior to these treatments, each compound underwent dose-response
671 assays using serial dilutions to determine the highest concentration that was both nontoxic and effective. The
672 optimal concentrations identified were used in all subsequent experiments and are detailed in Supplementary
673 Table 6.

674 For *in vivo* experiments, compounds were dissolved in a 50:50 (v/v) ethanol/sesame oil mixture and
675 topically applied daily to the dorsal skin of K14-Kitl mice for 2 weeks. Control mice received the vehicle
676 solution without compound. Dose-response assays were conducted beforehand to establish the highest

677 nontoxic and effective concentrations, which were then used in all experiments. The final working
678 concentrations are listed in Supplementary Table 7.

679 For *ex vivo* experiments, skin explants were maintained for 1 week in DMEM supplemented with 10%
680 fetal bovine serum and 1% penicillin-streptomycin. The culture medium, containing the respective
681 compounds or DMSO vehicle, was replaced every 2 days. Prior dose-response assays determined the optimal
682 nontoxic and effective concentrations for each compound, which were subsequently used in all experiments.
683 These concentrations are provided in Supplementary Table 8.

684 **Statistical analysis**

685 All experiments were repeated at least three times, and results are presented as the mean ± standard
686 deviation. Statistical analyses were performed using unpaired two-tailed Student's t-tests, one-way analysis
687 of variance (ANOVA) with Dunnett's *post hoc* test, or two-way ANOVA, as appropriate. The same statistical
688 approach was applied to both *in vitro* and *in vivo* data. Statistical significance was defined as $P < 0.05$. All
689 analyses were carried out using GraphPad Prism v9.5.3 (GraphPad Software, Boston, MA, USA).

690 **Data availability**

691 The data that support the findings of this study are available from the corresponding author upon
692 reasonable request.

693 **Acknowledgments**

694 We gratefully acknowledge Hideki Nakagawa of the Research Support Platform at Osaka Metropolitan
695 University Graduate School of Medicine for providing expert technical assistance with electron microscopy.

696 **Figure legends**

697 **Figure 1. Distinct adhesion profiles of melanocytes in healthy and vitiliginous skin**

698 **a**. Immunofluorescence analysis of laminin isoform distribution in healthy control skin and perilesional
699 vitiligo skin (Vitiligo-PL). Laminin-211 (LN211) components include α2, β1, and γ1 chains; laminin-332
700 (LN332) components include α3, β3, and γ2 chains. Melanocytes are indicated by white arrows. Scale bar:
701 5 μm. **b**. Immuno-electron microscopy using anti-laminin α3 (LNα3) antibody reveals ultrastructural
702 localization of laminin-332 around melanocytes in healthy and vitiligo-PL skin. Scale bar: 1 μm. **c**. Schematic
703 of proximity ligation assay (PLA) for detecting protein-protein interactions between melanocyte surface
704 receptors (e.g., DG, ITGβ1, DDR1) and basement membrane components (e.g., LNα2, LN332, LNα5, Col4).
705 Melanocytes are costained using anti-c-Kit antibody. BM, basement membrane; MC, melanocyte. **d**.
706 Representative PLA images showing red fluorescent signals (PLA puncta) indicating protein-protein
707 interactions in healthy and vitiligo-PL skin. Costaining with c-Kit identifies melanocytes (green); nuclei are
708 counterstained with 4′,6-diamidino-2-phenylindole (DAPI; blue). Scale bar: 50 μm. **e**. Proposed model of
709 melanocyte-basement membrane (MC-BM) adhesion patterns in healthy and vitiligo-PL skin. **f**. Functional
710 validation of DG-mediated melanocyte adhesion to LN211-coated plates using antibody blockade, small
711 interfering RNA (siRNA) knockdown, and enzymatic deglycosylation. Scale bar: 500 μm. Ab, antibody;
712 PBS, phosphate-buffered saline.

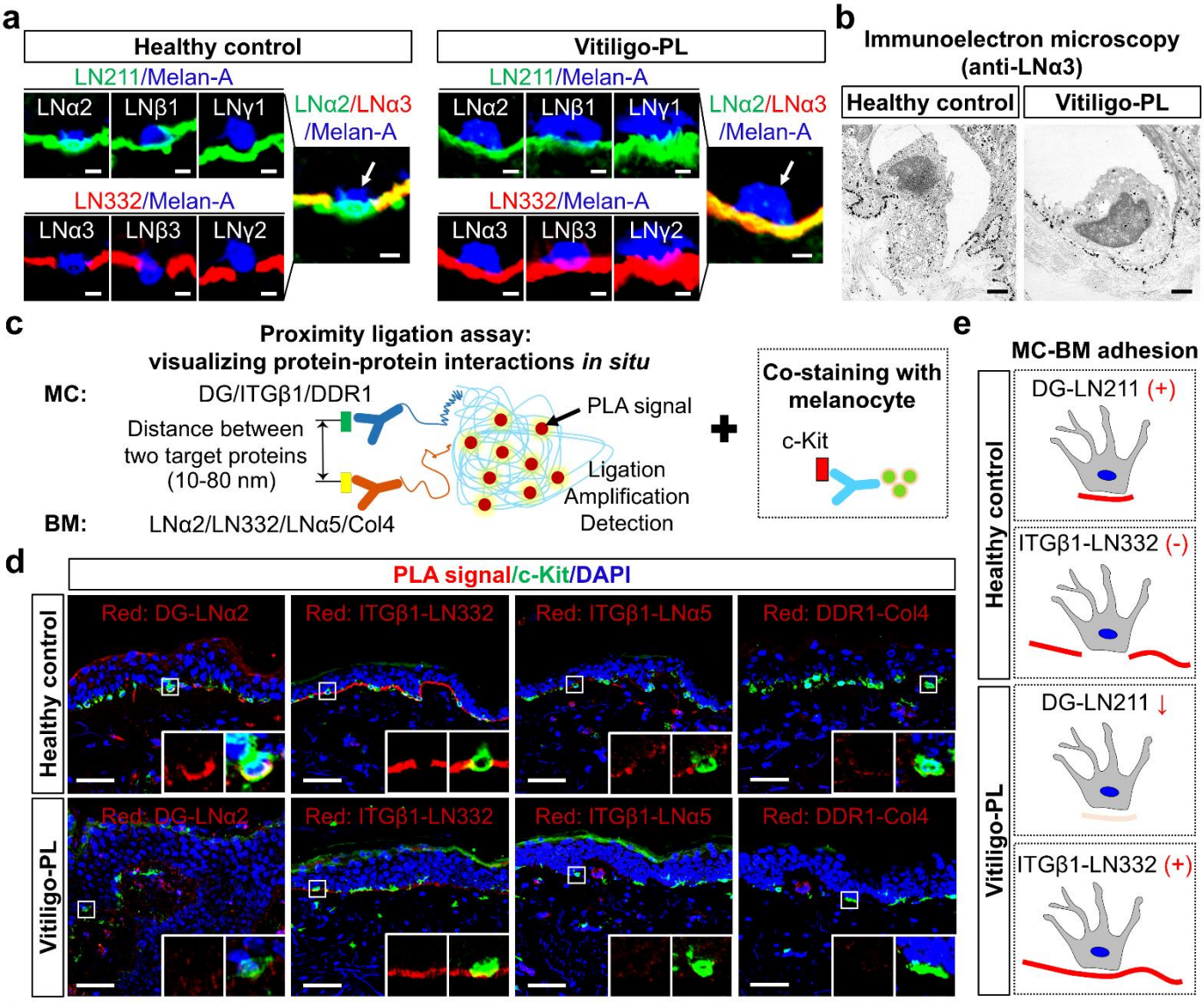
a
Healthy control
Vitiligo-PL
LN211/Melan-A
LNα2
LNβ1
LNγ1
LNα2/LNα3
/Melan-A
LN332/Melan-A
LNα3
LNβ3
LNγ2
b
Immunoelectron microscopy
(anti-LNα3)
Healthy control
Vitiligo-PL
c
Proximity ligation assay:
visualizing protein-protein interactions in situ
MC:
DG/ITGβ1/DDR1
Distance between
two target proteins
(10-80 nm)
BM:
LNα2/LN332/LNα5/Col4
PLA signal
Ligation
Amplification
Detection
Co-staining with
melanocyte
c-Kit
e
MC-BM adhesion
Healthy control
DG-LN211 (+)
ITGβ1-LN332 (-)
Vitiligo-PL
DG-LN211 ↓
ITGβ1-LN332 (+)
d
PLA signal/c-Kit/DAPI
Healthy control
Vitiligo-PL
Red: DG-LNα2
Red: ITGβ1-LN332
Red: ITGβ1-LNα5
Red: DDR1-Col4
f
Adhesion of melanocytes in plates coated with LN211
Antibody blockade
siRNA knockdown
Enzymatic deglycosylation
IgG-Ab
DG-Ab
ITGβ1-Ab
ITGα7-Ab
siMOCK
siDG
siLARGE
siITGβ1
PBS
O-glycosidase
(0.3 U/ml)
O-glycosidase
(0.15 U/ml)
O-glycosidase
(0.075 U/ml)

713

714 **Figure 2. Laminin-332 induces dedifferentiation in human melanocytes**

715 **a.** Morphological and phenotypic changes of melanocytes cultured on plates coated with laminin-211
716 (LN211) or laminin-332 (LN332). Cells were stained with phalloidin (F-actin, blue), PMEL17 (green), and
717 TYRP1 (red). Merged images demonstrate reduced expression of melanocytic markers and altered cell
718 morphology under LN332-coated conditions. Scale bar: 100 μm. **b.** Quantification of c-Kit-positive and c-
719 Kit-negative melanocytes after magnetic-activated cell sorting (MACS) under LN211- and LN332-coated
720 conditions. Data are shown as mean ± SD. Western blot (WB) analysis of melanocyte lineage markers in
721 cells cultured on LN211 or LN332 substrates, with c-Kit-based MACS. Analyzed proteins include c-Kit,
722 tyrosinase (TYR), Melan-A, TYRP1, PMEL17, and DCT. Glyceraldehyde 3-phosphate dehydrogenase
723 (GAPDH) was used as a loading control. **d.** Quantification of protein expression levels shown in panel **c**.
724 Data represent mean ± SD. Statistical significance was assessed by unpaired two-tailed Student's t-test, and
725 *P* values are indicated. **e.** Representative images of cell lysates from melanocyte pellets following culture
726 under the indicated conditions. **f.** Quantification of melanin content from panel **e**, revealing a significant
727 decrease in melanin levels in LN332-cultured cells. Data are shown as mean ± SD; *P* values (shown on
728 graph) were calculated by one-way analysis of variance with Tukey's *post hoc* test. **g.** Gene set enrichment
729 analysis of melanocytes cultured on LN332, showing enrichment for embryonic stem cell and neural crest
730 cell gene signatures, indicating loss of lineage identity. **h.** Assessment of multilineage differentiation
731 potential in LN332-treated melanocytes. Cells were subjected to lineage-specific induction protocols and
732 immunostained for neurofilament (neuronal), collagen II (chondrogenic), and alpha-smooth muscle actin (α-
733 SMA; myogenic) markers. Scale bar: 100 μm. DAPI, 4′,6-diamidino-2-phenylindole.

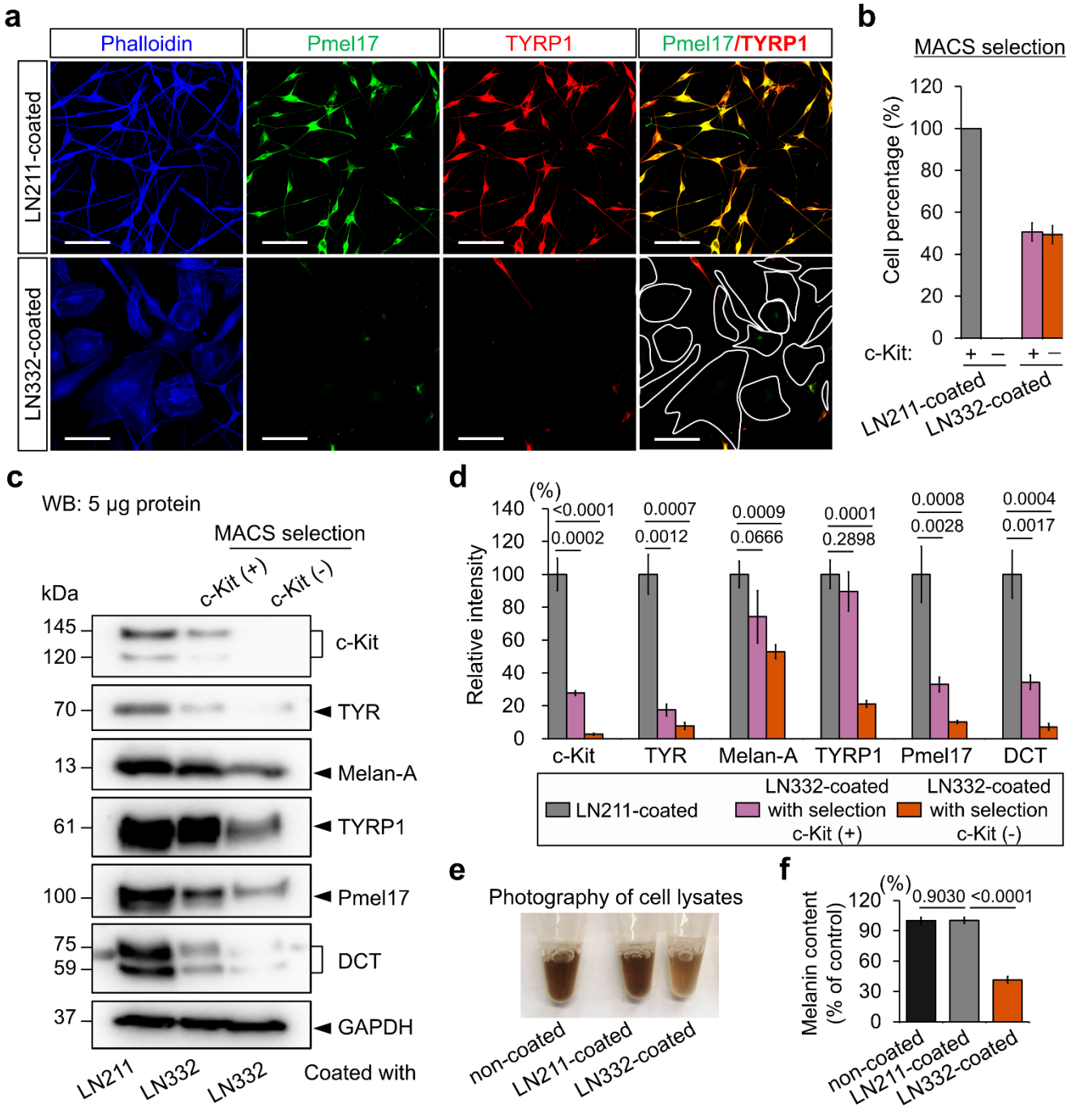
a
Phalloidin
Pmel17
TYRP1
Pmel17/TYRP1
LN211-coated
LN332-coated
b
MACS selection
Cell percentage (%)
120
100
80
60
40
20
0
c-Kit:
+ −
+ −
LN211-coated
LN332-coated
c
WB: 5 µg protein
MACS selection
c-Kit (+)
c-Kit (-)
kDa
145
120
c-Kit
70
TYR
13
Melan-A
61
TYRP1
100
Pmel17
75
59
DCT
37
GAPDH
LN211
LN332
LN332
Coated with
d
(%)
Relative intensity
140
120
100
80
60
40
20
0
<0.0001
0.0002
0.0007
0.0012
0.0009
0.0666
0.0001
0.2898
0.0008
0.0028
0.0004
0.0017
c-Kit
TYR
Melan-A
TYRP1
Pmel17
DCT
LN211-coated
LN332-coated with selection c-Kit (+)
LN332-coated with selection c-Kit (-)
e
Photography of cell lysates
non-coated
LN211-coated
LN332-coated
f
(%)
Melanin content (% of control)
120
90
60
30
0
0.9030
<0.0001
non-coated
LN211-coated
LN332-coated
g
Embryonic Stem Cell
Enrichment score
0.6
0.4
0.2
0.0
NES = 1.88
p = 0
Neural Crest Cell
0.6
0.4
0.2
0.0
NES = 1.96
p = 0
h
Differentiation assay
DAPI
Neurofilament /Phalloidin/DAPI
Collagen II/DAPI
αSMA/DAPI
LN211-coated
LN332-coated

734

735 **Figure 3. Molecular mechanisms underlying laminin-332-induced dedifferentiation in melanocytes**

736 **a.** Volcano plot showing differentially expressed genes in melanocytes cultured on laminin-332 (LN332)
737 compared with laminin-211 (LN211), based on bulk RNA-seq analysis. Thresholds: $|\log_2 \text{fold change}| > 1$
738 and false discovery rate < 0.05. **b.** Gene ontology enrichment analysis of upregulated pathways in LN332-
739 treated melanocytes. Enriched signaling pathways include PI3K-Akt, MAPK, focal adhesion, and Hippo
740 signaling. **c.** Representative immunofluorescence images of melanocytes after small interfering RNA
741 (siRNA)-mediated knockdown of YAP1, c-Jun, ERK1, and CTNNB1 (β-catenin). Cells were stained for
742 Melan-A (red) and nuclei (4′,6-diamidino-2-phenylindole, DAPI; blue). Scale bar: 100 μm. **d.** Quantification
743 of mature melanocyte populations after gene knockdown. Data represent mean ± SD. Statistical significance
744 was assessed using one-way analysis of variance with *post hoc* testing. ***$P < 0.001$; n.s., not significant. **e.**
745 Rescue of melanocyte differentiation on noncoated plates *via* cotreatment with pathway activators and
746 inhibitors. Representative images showing the effect of JNK inhibition (SP600125) on cells treated with
747 Rho/Rac/Cdc42 activator or PY-60 (YAP activator). Scale bar: 100 μm. DMSO, dimethyl sulfoxide. **f-h.**
748 Quantification of melanocyte differentiation under various pathway-modulator treatments corresponding to
749 panels **e** and **g**. Data are shown as mean ± SD; ***$P < 0.001$; n.s., not significant. **g.** Rescue of melanocyte
750 differentiation on LN332-coated plates using inhibitors targeting the MAPK pathway, including BRAF, MEK,
751 p38, ERK, and JNK. Cells were stained for Melan-A (red) and nuclei (DAPI, blue). Scale bar: 100 μm.

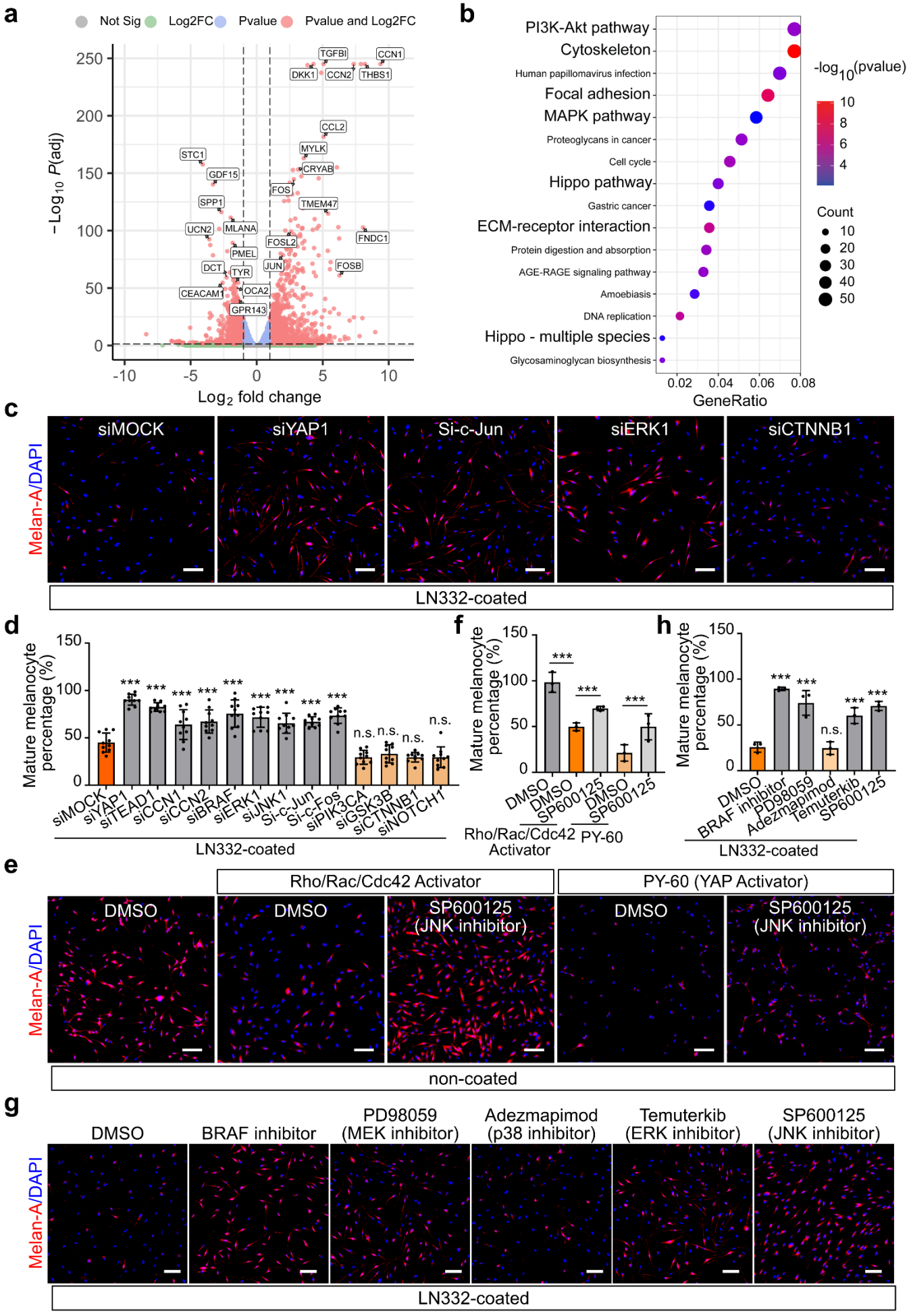
a
Not Sig
Log2FC
Pvalue
Pvalue and Log2FC
−Log10 P(adj)
Log2 fold change
TGFBI
CCN1
DKK1
CCN2
THBS1
CCL2
MYLK
CRYAB
STC1
GDF15
FOS
SPP1
TMEM47
UCN2
MLANA
FOSL2
FNDC1
PMEL
DCT
TYR
JUN
FOSB
CEACAM1
OCA2
GPR143
b
PI3K-Akt pathway
Cytoskeleton
Human papillomavirus infection
Focal adhesion
MAPK pathway
Proteoglycans in cancer
Cell cycle
Hippo pathway
Gastric cancer
ECM-receptor interaction
Protein digestion and absorption
AGE-RAGE signaling pathway
Amoebiasis
DNA replication
Hippo - multiple species
Glycosaminoglycan biosynthesis
GeneRatio
-log10(pvalue)
Count
c
siMOCK
siYAP1
Si-c-Jun
siERK1
siCTNNB1
Melan-A/DAPI
LN332-coated
d
Mature melanocyte percentage (%)
siMOCK
siYAP1
siTEAD1
siCCN1
siCCN2
siBRAF
siERK1
siJNK1
Si-c-Jun
Si-c-Fos
siPIK3CA
siGSK3B
siCTNNB1
siNOTCH1
LN332-coated
f
Mature melanocyte percentage (%)
DMSO
DMSO
SP600125
DMSO
SP600125
Rho/Rac/Cdc42 Activator
PY-60
h
Mature melanocyte percentage (%)
DMSO
BRAF inhibitor
PD98059
Adezmapimod
Temuterkib
SP600125
LN332-coated
e
Rho/Rac/Cdc42 Activator
PY-60 (YAP Activator)
DMSO
DMSO
SP600125 (JNK inhibitor)
DMSO
SP600125 (JNK inhibitor)
Melan-A/DAPI
non-coated
g
DMSO
BRAF inhibitor
PD98059 (MEK inhibitor)
Adezmapimod (p38 inhibitor)
Temuterkib (ERK inhibitor)
SP600125 (JNK inhibitor)
Melan-A/DAPI
LN332-coated

752

753 **Figure 4. Validation of Rho/Hippo/MAPK pathway involvement in melanocyte differentiation across**
754 **multiple models**

755 **a.** *In vitro* effects of pathway modulation on melanocyte differentiation. Human melanocytes were cultured
756 on plates coated with laminin-332 (LN332) and treated with specific inhibitors or activators targeting the
757 Rho/F-actin cytoskeleton, Hippo (YAP), or MAPK (JNK) pathways for 24 hours. Cells were stained with
758 anti-Melan-A (red) and phalloidin (F-actin; blue). Scale bar: 100 μm. DMSO, dimethyl sulfoxide. **b.** *In vivo*
759 validation using K14-Kitl mice subjected to topical treatment with pathway modulators for 2-4 weeks. Top
760 panels: bright-field images of dorsal skin sections showing pigmentation status. Middle panels:
761 immunofluorescence staining for mature melanocytes using anti-TYRP1 (red) and anti-collagen IV (blue).
762 Bottom panels: staining for immature melanocytes using anti-c-Kit (green) and anti-collagen IV (blue). c-
763 Kit single-positive cells located in the epidermis were defined as immature melanocytes. Scale bar: 50 μm
764 (immunofluorescence), 100 μm (bright-field). **c.** *Ex vivo* human skin explant model treated with pathway
765 modulators for 1 week. Top panels: 3,4-dihydroxyphenylalanine (DOPA) staining visualizing functionally
766 mature melanocytes. Bottom panels: immunofluorescence staining for mature melanocytes (Melan-A, red;
767 collagen IV, blue). Scale bar: 100 μm (DOPA), 50 μm (immunofluorescence).

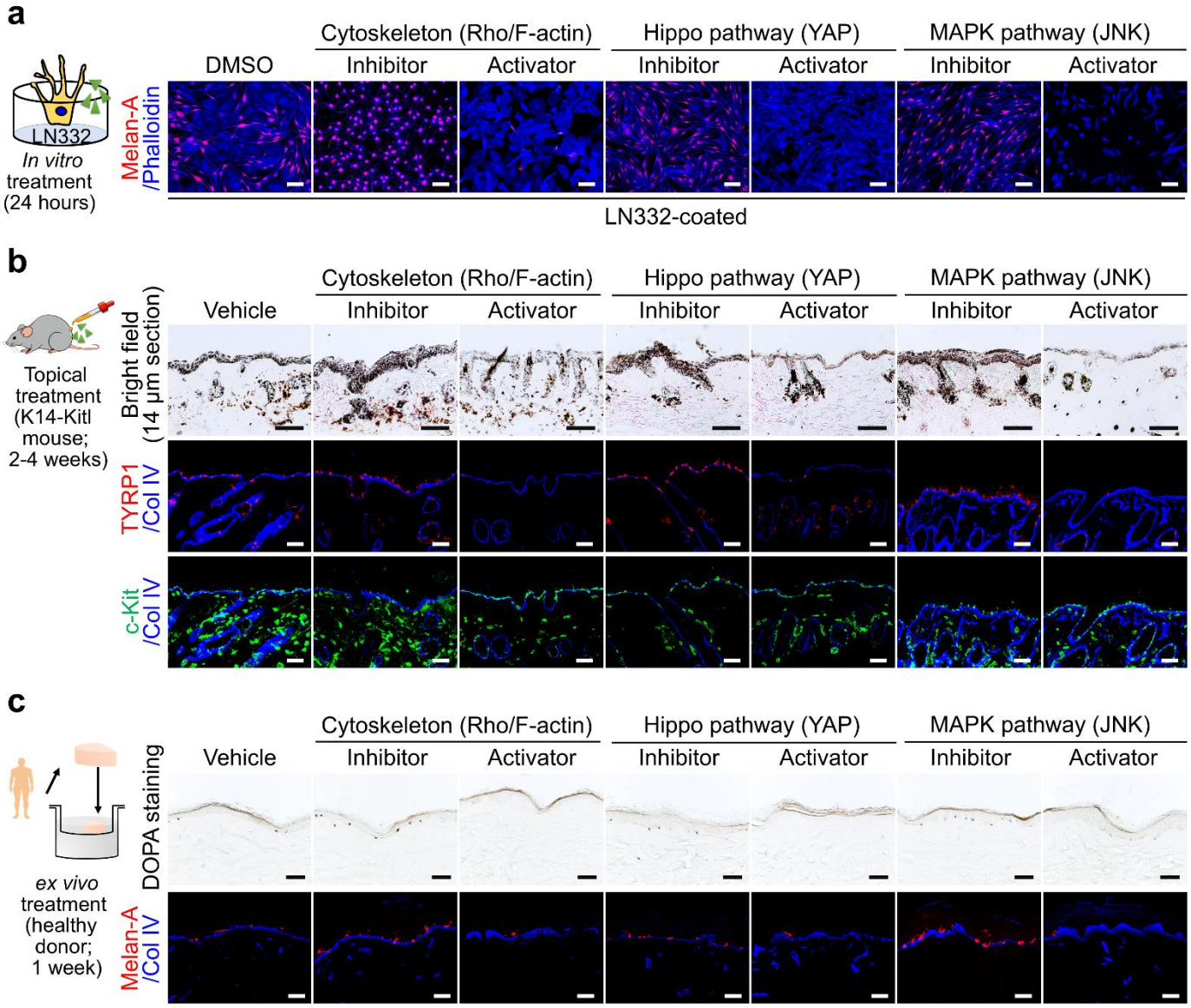
a
Cytoskeleton (Rho/F-actin)
Hippo pathway (YAP)
MAPK pathway (JNK)
DMSO
Inhibitor
Activator
Inhibitor
Activator
Inhibitor
Activator
LN332
In vitro treatment (24 hours)
Melan-A /Phalloidin
LN332-coated
b
Cytoskeleton (Rho/F-actin)
Hippo pathway (YAP)
MAPK pathway (JNK)
Vehicle
Inhibitor
Activator
Inhibitor
Activator
Inhibitor
Activator
Topical treatment (K14-Kitl mouse; 2-4 weeks)
Bright field (14 µm section)
TYRP1 /Col IV
c-Kit /Col IV
c
Cytoskeleton (Rho/F-actin)
Hippo pathway (YAP)
MAPK pathway (JNK)
Vehicle
Inhibitor
Activator
Inhibitor
Activator
Inhibitor
Activator
ex vivo treatment (healthy donor; 1 week)
DOPA staining
Melan-A /Col IV

768

769 **Figure 5. Evidence of melanocyte dedifferentiation in skin from patients with vitiligo**

770 **a.** 3,4-dihydroxyphenylalanine (DOPA) staining of healthy control and perilesional vitiligo (Vitiligo-PL)
771 skin reveals reduced melanocyte function in vitiliginous areas. Scale bar: 100 μm. **b.** Immunofluorescence
772 analysis of melanocyte markers in healthy and Vitiligo-PL skin. Staining includes DCT (green), SOX9
773 (green), F-actin (green), p-c-Jun (green), Melan-A (red), and 4′,6-diamidino-2-phenylindole (DAPI; blue).
774 Insets highlight melanocytes with altered marker expression patterns in Vitiligo-PL samples. Scale bar: 50
775 μm. **c.** Overexpression (OE) of SOX9 in cultured melanocytes (SOX9-OE) enhances melanocyte
776 dedifferentiation. Cells were stained for SOX9 (green), His-tag (red), and Melan-A (blue). Enlarged view
777 highlights SOX9/His-tag positive cells with low Melan-A expression. Scale bar: 100 μm. **d.** SOX9
778 knockdown by small interfering RNA (siRNA; siSOX9) promotes melanocyte differentiation in cultured
779 melanocytes. Cells were stained for SOX9 (green), Melan-A (red), and phalloidin (blue). Scale bar: 100 μm.
780 **e.** Spatial transcriptomics of perilesional vitiligo skin identifies two melanocyte populations: mature
781 differentiated melanocytes (MC; $PMEL^{+}$/$MLANA^{+}$/$TYRP1^{+}$/$MITF^{+}$/DCT^{+}/$SOX10^{+}$) and dedifferentiating
782 or dedifferentiated melanocytes (DeMC; $MLANA^{-}$/DCT^{+}, $SOX9^{+}$ or $NGFR^{+}$). Gene expression heatmap
783 ($\log_2$ fold change) highlights upregulation of dedifferentiation-related genes (*SOX9*, *NGFR*, *YAP1*, *RHOV*,
784 *JUN* family) in DeMC, and loss of pigment genes (*TYRP1*, *MLANA*, *MITF*) compared with MC.

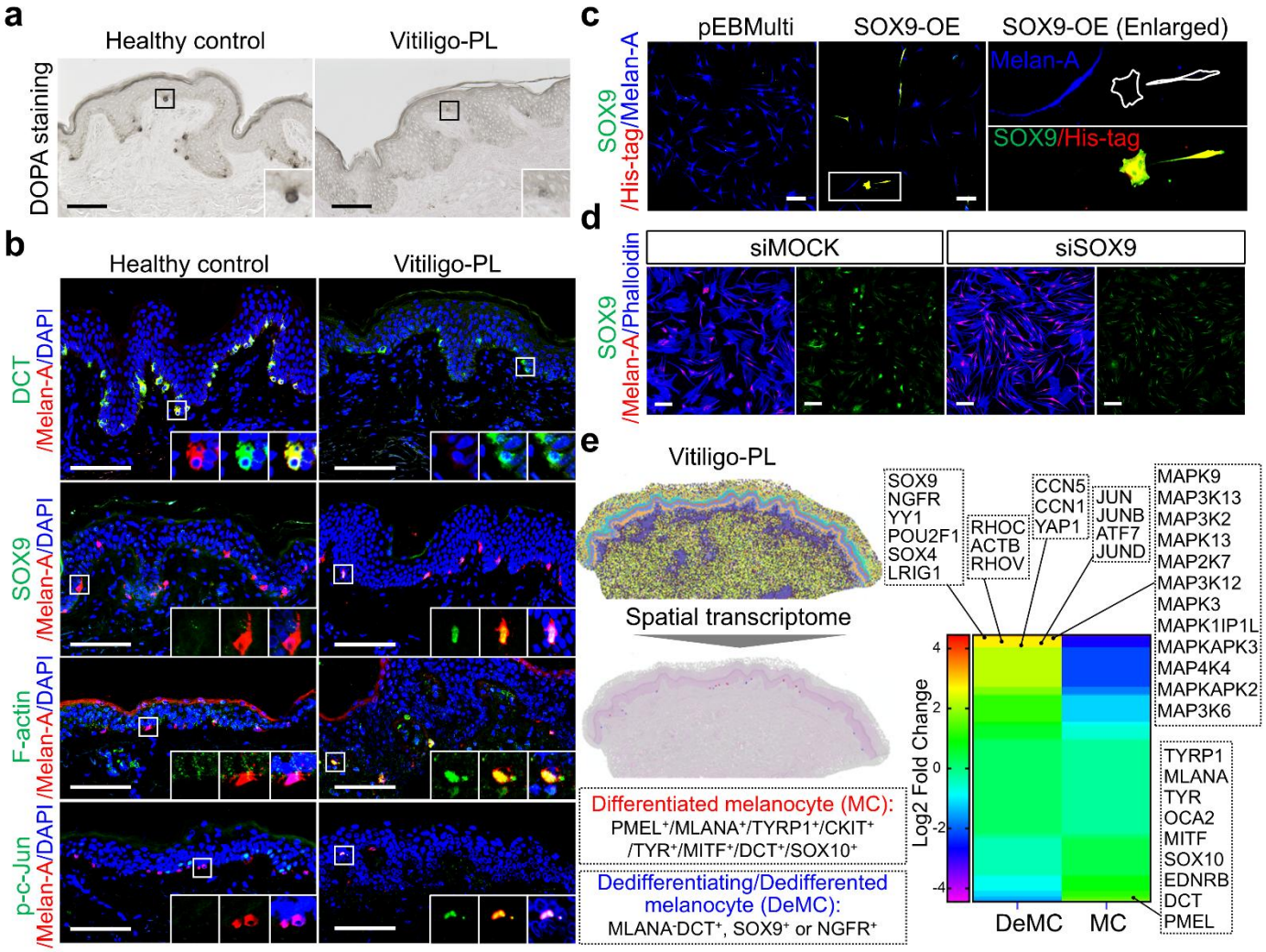
a
Healthy control
Vitiligo-PL
DOPA staining
b
Healthy control
Vitiligo-PL
DCT /Melan-A/DAPI
SOX9 /Melan-A/DAPI
F-actin /Melan-A/DAPI
p-c-Jun /Melan-A/DAPI
c
pEBMulti
SOX9-OE
SOX9-OE (Enlarged)
SOX9 /His-tag/Melan-A
Melan-A
SOX9/His-tag
d
siMOCK
siSOX9
SOX9 /Melan-A/Phalloidin
e
Vitiligo-PL
Spatial transcriptome
Differentiated melanocyte (MC):
PMEL+/MLANA+/TYRP1+/CKIT+
/TYR+/MITF+/DCT+/SOX10+
Dedifferentiating/Dedifferented
melanocyte (DeMC):
MLANA-DCT+, SOX9+ or NGFR+
SOX9
NGFR
YY1
POU2F1
SOX4
LRIG1
RHOC
ACTB
RHOV
CCN5
CCN1
YAP1
JUN
JUNB
ATF7
JUND
MAPK9
MAP3K13
MAP3K2
MAPK13
MAP2K7
MAP3K12
MAPK3
MAPK1IP1L
MAPKAPK3
MAP4K4
MAPKAPK2
MAP3K6
TYRP1
MLANA
TYR
OCA2
MITF
SOX10
EDNRB
DCT
PMEL
Log2 Fold Change
4
2
0
-2
-4
DeMC
MC

785

786

787 **Figure 6. Therapeutic efficacy of dedifferentiation-targeted therapy in vitiligo models**

788 **a.** Dose-dependent effects of laminin-332 (LN332) on pigmentation in a three-dimensional (3D)
789 reconstructed human skin model. LN332 was applied at increasing concentrations (0-20 μg/mL), resulting
790 in progressive pigment loss in a concentration-dependent manner. **b.** Localized pigment loss induced by
791 LN332 in a custom-designed culture chamber. Melanocytes cultured on LN332-coated areas exhibited
792 patterned depigmentation. **c.** Rescue of pigmentation in the 3D skin model following treatment with the
793 dedifferentiation inhibitor SP600125 (a JNK inhibitor). Cells were stained for Melan-A (green) and nuclei
794 (4′,6-diamidino-2-phenylindole, DAPI; blue). Scale bar: 50 μm. DMSO, dimethyl sulfoxide. **d.** *In vivo*
795 therapeutic effect of dedifferentiation inhibitors in a rhododendrol-induced leukoderma mouse model (K14-
796 Kitl mice). Skin pigmentation was assessed by dermoscopy and bright-field imaging. Immunofluorescence
797 staining for TYRP1 (red) and LNγ2 (blue) demonstrated restored melanocyte differentiation and
798 pigmentation following SP600125 treatment. Scale bar: 100 μm. **e.** *Ex vivo* treatment with SP600125 for 1
799 week of perilesional vitiligo skin from patients. **f.** 3,4-dihydroxyphenylalanine (DOPA) staining and
800 immunofluorescence analysis of treated human skin explants. SP600125 restored functional melanocytes, as
801 indicated by increased pigmentation and Melan-A expression (red). Collagen IV is shown in green, and DAPI
802 in blue. Scale bar: 200 μm. **g.** Schematic illustration of melanocyte states in healthy versus vitiligo skin,
803 illustrating the transition from differentiated to dedifferentiated states and the therapeutic reversal by
804 dedifferentiation inhibition.

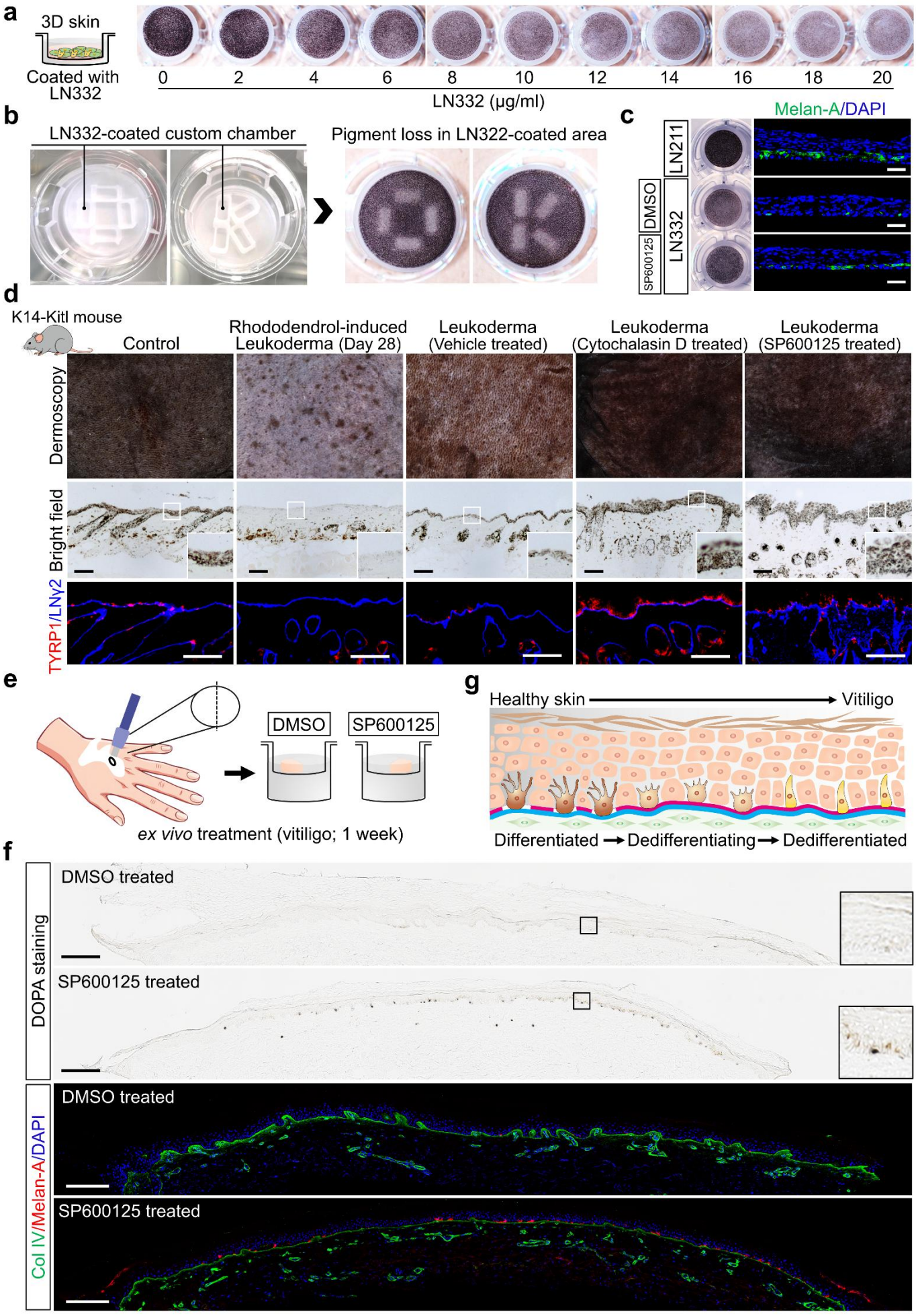
a
3D skin
Coated with LN332
0
2
4
6
8
10
12
14
16
18
20
LN332 (μg/ml)
b
LN332-coated custom chamber
Pigment loss in LN322-coated area
c
Melan-A/DAPI
LN211
DMSO
LN332
SP600125
d
K14-Kitl mouse
Control
Rhododendrol-induced Leukoderma (Day 28)
Leukoderma (Vehicle treated)
Leukoderma (Cytochalasin D treated)
Leukoderma (SP600125 treated)
Dermoscopy
Bright field
TYRP1/LNγ2
e
DMSO
SP600125
ex vivo treatment (vitiligo; 1 week)
g
Healthy skin
Vitiligo
Differentiated
Dedifferentiating
Dedifferentiated
f
DOPA staining
DMSO treated
SP600125 treated
Col IV/Melan-A/DAPI
DMSO treated
SP600125 treated

806 **References**

807 1. Bibeau, K., *et al.* Mental Health and Psychosocial Quality-of-Life Burden Among Patients With Vitiligo: Findings From the
808 Global VALIANT Study. *JAMA dermatology* **159**, 1124-1128 (2023).
809 2. van den Boorn, J.G., *et al.* Autoimmune destruction of skin melanocytes by perilesional T cells from vitiligo patients. *J.*
810 *Invest. Dermatol.* **129**, 2220-2232 (2009).
811 3. Abdel-Malek, Z.A., *et al.* The enigma and challenges of vitiligo pathophysiology and treatment. *Pigment cell & melanoma*
812 *research* **33**, 778-787 (2020).
813 4. Jian, Z., *et al.* Impaired activation of the Nrf2-ARE signaling pathway undermines H2O2-induced oxidative stress response:
814 a possible mechanism for melanocyte degeneration in vitiligo. *J. Invest. Dermatol.* **134**, 2221-2230 (2014).
815 5. Boukhedouni, N., *et al.* Type-1 cytokines regulate MMP-9 production and E-cadherin disruption to promote melanocyte
816 loss in vitiligo. *JCI Insight* **5**(2020).
817 6. Wagner, R.Y., *et al.* Altered E-Cadherin Levels and Distribution in Melanocytes Precede Clinical Manifestations of Vitiligo.
818 *J. Invest. Dermatol.* **135**, 1810-1819 (2015).
819 7. Gauthier, Y., Cario-Andre, M., Lepreux, S., Pain, C. & Taieb, A. Melanocyte detachment after skin friction in non lesional
820 skin of patients with generalized vitiligo. *Br. J. Dermatol.* **148**, 95-101 (2003).
821 8. Bastonini, E., *et al.* A protective role for autophagy in vitiligo. *Cell Death Dis.* **12**, 318 (2021).
822 9. Bellei, B., *et al.* Vitiligo: a possible model of degenerative diseases. *PLoS One* **8**, e59782 (2013).
823 10. Tobin, D.J., Swanson, N.N., Pittelkow, M.R., Peters, E.M. & Schallreuter, K.U. Melanocytes are not absent in lesional skin
824 of long duration vitiligo. *J. Pathol.* **191**, 407-416 (2000).
825 11. Husain, I., Vijayan, E., Ramaiah, A., Pasricha, J.S. & Madan, N.C. Demonstration of tyrosinase in the vitiligo skin of human
826 beings by a sensitive fluorometric method as well as by 14C(U)-L-tyrosine incorporation into melanin. *J. Invest. Dermatol.*
827 **78**, 243-252 (1982).
828 12. Lin, J.Y. & Fisher, D.E. Melanocyte biology and skin pigmentation. *Nature* **445**, 843-850 (2007).
829 13. Yang, F., *et al.* Disorganisation of basement membrane zone architecture impairs melanocyte residence in vitiligo. *The*
830 *Journal of pathology* **264**, 30-41 (2024).
831 14. Panuncio, A.L. & Vignale, R. Ultrastructural studies in stable vitiligo. *Am. J. Dermatopathol.* **25**, 16-20 (2003).
832 15. Fawzy, M.M., El Maadawi, Z.M., Hegazy, R.A. & El Fatah, N.S. Vitiligo - The story from within: A transmission electron
833 microscopic study before and after narrow-band ultraviolet B. *Ultrastruct. Pathol.* **40**, 265-275 (2016).
834 16. Montes, L.F., Abulafia, J., Wilborn, W.H., Hyde, B.M. & Montes, C.M. Value of histopathology in vitiligo. *Int. J. Dermatol.*
835 **42**, 57-61 (2003).
836 17. Breathnach, A.S., Bor, S. & Wyllie, L.M. Electron microscopy of peripheral nerve terminals and marginal melanocytes in
837 vitiligo. *J. Invest. Dermatol.* **47**, 125-140 (1966).
838 18. Luthold, C., *et al.* Melanocyte differentiation and mechanosensation are differentially modulated by distinct extracellular
839 matrix proteins. *bioRxiv*, 2024.2010.2004.616635 (2024).
840 19. Ranson, M., Posen, S. & Mason, R.S. Extracellular matrix modulates the function of human melanocytes but not
841 melanoma cells. *Journal of cellular physiology* **136**, 281-288 (1988).
842 20. Hedley, S., Gawkrodger, D.J., Weetman, A.P. & MacNeil, S. Investigation of the influence of extracellular matrix proteins
843 on normal human melanocyte morphology and melanogenic activity. *The British journal of dermatology* **135**, 888-897
844 (1996).
845 21. Shibata, S., *et al.* Selective Laminin-Directed Differentiation of Human Induced Pluripotent Stem Cells into Distinct Ocular
846 Lineages. *Cell Rep.* **25**, 1668-1679 e1665 (2018).
847 22. Yap, L., Tay, H.G., Nguyen, M.T.X., Tjin, M.S. & Tryggvason, K. Laminins in Cellular Differentiation. *Trends Cell Biol.* **29**, 987-
848 1000 (2019).
849 23. Hall, M.L., *et al.* Laminin 411 mediates endothelial specification via multiple signaling axes that converge on beta-catenin.

850 *Stem Cell Reports* **17**, 569-583 (2022).
851 24. Ricard, A.S.*, et al.* Study of CCN3 (NOV) and DDR1 in normal melanocytes and vitiligo skin. *Exp. Dermatol.* **21**, 411-416
852 (2012).
853 25. Fukunaga-Kalabis, M.*, et al.* CCN3 controls 3D spatial localization of melanocytes in the human skin through DDR1. *J. Cell*
854 *Biol.* **175**, 563-569 (2006).
855 26. Zambruno, G.*, et al.* Expression of integrin receptors and their role in adhesion, spreading and migration of normal
856 human melanocytes. *J. Cell Sci.* **105 (Pt 1)**, 179-190 (1993).
857 27. Yamada, M. & Sekiguchi, K. Chapter Six - Molecular Basis of Laminin–Integrin Interactions. in *Current Topics in*
858 *Membranes*, Vol. 76 (ed. Miner, J.H.) 197-229 (Academic Press, 2015).
859 28. Arimori, T.*, et al.* Structural mechanism of laminin recognition by integrin. *Nat Commun* **12**, 4012 (2021).
860 29. Sugawara, K., Tsuruta, D., Ishii, M., Jones, J.C. & Kobayashi, H. Laminin-332 and -511 in skin. *Exp. Dermatol.* **17**, 473-480
861 (2008).
862 30. Zhong, Z., Jiao, Z. & Yu, F.-X. The Hippo signaling pathway in development and regeneration. *Cell reports* **43**(2024).
863 31. Renshaw, M.W., Toksoz, D. & Schwartz, M.A. Involvement of the small GTPase rho in integrin-mediated activation of
864 mitogen-activated protein kinase. *The Journal of biological chemistry* **271**, 21691-21694 (1996).
865 32. Koo, J.H. & Plouffe, S.W. Induction of AP-1 by YAP/TAZ contributes to cell proliferation and organ growth. **34**, 72-86 (2020).
866 33. Whitmarsh, A.J. & Davis, R.J. Transcription factor AP-1 regulation by mitogen-activated protein kinase signal transduction
867 pathways. *J. Mol. Med. (Berl.)* **74**, 589-607 (1996).
868 34. Du, M., Liu, M., Fan, F., Shi, P. & Tu, M. Structure, Function, and Nutrition of Lactoferrin. in *Mineral Containing Proteins :*
869 *Roles in Nutrition* (ed. Zhao, G.) 33-61 (Springer Singapore, Singapore, 2017).
870 35. Moretti, S.*, et al.* New insights into the pathogenesis of vitiligo: imbalance of epidermal cytokines at sites of lesions.
871 *Pigment Cell Res.* **15**, 87-92 (2002).
872 36. Passi, S., Grandinetti, M., Maggio, F., Stancato, A. & De Luca, C. Epidermal oxidative stress in vitiligo. *Pigment Cell Res.*
873 **11**, 81-85 (1998).
874 37. Xu, P.*, et al.* Effects of EGFR-TKI on epidermal melanin unit integrity: Therapeutic implications for hypopigmented skin
875 disorders. *Pigment cell & melanoma research* **37**, 514-529 (2024).
876 38. Horvai, A.E.*, et al.* Nuclear integration of JAK/STAT and Ras/AP-1 signaling by CBP and p300. *Proc. Natl. Acad. Sci. U. S. A.*
877 **94**, 1074-1079 (1997).
878 39. Kyriakis, J.M. & Avruch, J. Mammalian MAPK signal transduction pathways activated by stress and inflammation: a 10-
879 year update. *Physiol. Rev.* **92**, 689-737 (2012).
880 40. Katz, M., Amit, I. & Yarden, Y. Regulation of MAPKs by growth factors and receptor tyrosine kinases. *Biochim. Biophys.*
881 *Acta* **1773**, 1161-1176 (2007).
882 41. Loftus, S.K.*, et al.* Comparison of melanoblast expression patterns identifies distinct classes of genes. *Pigment cell &*
883 *melanoma research* **22**, 611-622 (2009).
884 42. Mort, R.L., Jackson, I.J. & Patton, E.E. The melanocyte lineage in development and disease. *Development* **142**, 620-632
885 (2015).
886 43. Cook, A.L., Smith, A.G., Smit, D.J., Leonard, J.H. & Sturm, R.A. Co-expression of SOX9 and SOX10 during melanocytic
887 differentiation in vitro. *Experimental cell research* **308**, 222-235 (2005).
888 44. Shakhova, O.*, et al.* Antagonistic cross-regulation between Sox9 and Sox10 controls an anti-tumorigenic program in
889 melanoma. *PLoS genetics* **11**, e1004877 (2015).
890 45. Harris, M.L., Baxter, L.L., Loftus, S.K. & Pavan, W.J. Sox proteins in melanocyte development and melanoma. *Pigment cell*
891 *& melanoma research* **23**, 496-513 (2010).
892 46. Stüfchen, I.*, et al.* Sox9 regulates melanocytic fate decision of adult hair follicle stem cells. *iScience* **26**, 106919 (2023).
893 47. Hedstrand, H.*, et al.* The Transcription Factors SOX9 and SOX10 Are Vitiligo Autoantigens in Autoimmune Polyendocrine
894 Syndrome Type I *. *Journal of Biological Chemistry* **276**, 35390-35395 (2001).
895 48. Zhu, S.*, et al.* GnRHa/Stanozolol Combined Therapy Maintains Normal Bone Growth in Central Precocious Puberty.
896 *Frontiers in endocrinology* **12**, 678797 (2021).

897 49. Inoue, S. & Katayama, I. Rhododendrol-induced leukoderma update II: Pathophysiology, mechanisms, risk evaluation,
898 and possible mechanism-based treatments in comparison with vitiligo. **48**, 969-978 (2021).
899 50. Sun, Q.*, et al.* Dedifferentiation maintains melanocyte stem cells in a dynamic niche. *Nature* **616**, 774-782 (2023).
900 51. Sbardella, D.*, et al.* α-dystroglycan is a potential target of matrix metalloproteinase MMP-2. *Matrix Biology* **41**, 2-7 (2015).
901 52. Pellegrini, C.*, et al.* Melanocytes--a novel tool to study mitochondrial dysfunction in Duchenne muscular dystrophy. *J.*
902 *Cell. Physiol.* **228**, 1323-1331 (2013).
903 53. Martin, P.T. The dystroglycanopathies: the new disorders of O-linked glycosylation. *Seminars in pediatric neurology* **12**,
904 152-158 (2005).
905 54. Yaar, M. & Park, H.-Y. Melanocytes: A Window into the Nervous System. *Journal of Investigative Dermatology* **132**, 835-
906 845 (2012).
907 55. Kumar, R., Parsad, D., Kanwar, A. & Kaul, D. Development of melanocye-keratinocyte co-culture model for controls and
908 vitiligo to assess regulators of pigmentation and melanocytes. *Indian journal of dermatology, venereology and leprology*
909 **78**, 599-604 (2012).
910 56. Kawakami, T. Surgical procedures and innovative approaches for vitiligo regenerative treatment and melanocytorrhagy.
911 *The Journal of dermatology* **49**, 391-401 (2022).
912 57. Kumar, R., Parsad, D., Kanwar, A.J. & Kaul, D. Altered levels of Ets-1 transcription factor and matrix metalloproteinases
913 in melanocytes from patients with vitiligo. *The British journal of dermatology* **165**, 285-291 (2011).
914 58. Robinson, R.L.*, et al.* Comparative STAT3-Regulated Gene Expression Profile in Renal Cell Carcinoma Subtypes. *Frontiers*
915 *in Oncology* **9**(2019).
916 59. Takahashi, K. & Yamanaka, S. Induction of pluripotent stem cells from mouse embryonic and adult fibroblast cultures by
917 defined factors. *Cell* **126**, 663-676 (2006).
918 60. Pesaresi, M., Sebastian-Perez, R. & Cosma, M.P. Dedifferentiation, transdifferentiation and cell fusion: in vivo
919 reprogramming strategies for regenerative medicine. *The FEBS Journal* **286**, 1074-1093 (2019).
920 61. Merrell, A.J. & Stanger, B.Z. Adult cell plasticity in vivo: de-differentiation and transdifferentiation are back in style.
921 *Nature Reviews Molecular Cell Biology* **17**, 413-425 (2016).
922 62. Shibata, S.*, et al.* Selective Laminin-Directed Differentiation of Human Induced Pluripotent Stem Cells into Distinct Ocular
923 Lineages. *Cell reports* **25**, 1668-1679.e1665 (2018).
924 63. Üstün, Y.*, et al.* Dual role of laminin-511 in regulating melanocyte migration and differentiation. *Matrix Biology* **80**, 59-
925 71 (2019).
926 64. Yui, S.*, et al.* YAP/TAZ-Dependent Reprogramming of Colonic Epithelium Links ECM Remodeling to Tissue Regeneration.
927 *Cell stem cell* **22**, 35-49.e37 (2018).
928 65. Manderfield, L.J.*, et al.* Pax3 and hippo signaling coordinate melanocyte gene expression in neural crest. *Cell reports* **9**,
929 1885-1895 (2014).
930 66. Tang, D.*, et al.* SRplot: A free online platform for data visualization and graphing. *PLoS One* **18**, e0294236 (2023).
931 67. Yang, F.*, et al.* Uncoupling of ER/Mitochondrial Oxidative Stress in mTORC1 Hyperactivation-Associated Skin
932 Hypopigmentation. *J. Invest. Dermatol.* **138**, 669-678 (2018).
933

Supplementary Information

Extended Data Figures

Extended Data Figure 1. Immunofluorescent staining of various laminin chains at the dermal-epidermal junction in normal human skin. Antibodies were used to detect pan-laminins (LNs), laminin α chains (LNα1-LNα5), laminin β chains (LNβ1-LNβ3), and laminin γ chains (LNγ1-LNγ3). Melanocytes were identified using a melanocyte-specific marker and are indicated by white arrowheads. Each panel displays the localization pattern of an individual laminin chain. Scale bar: 5 μm.

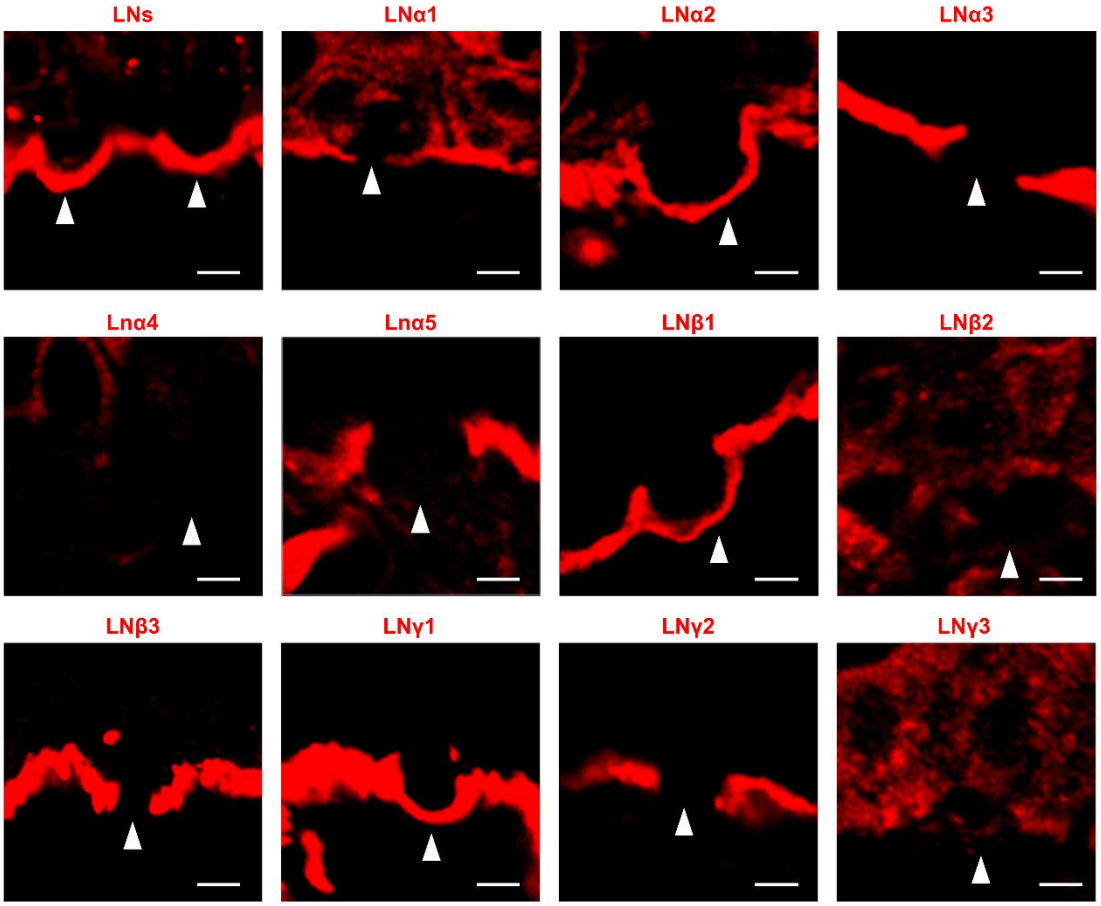

Extended Data Figure 2. Expression patterns of integrin subunits in normal human melanocytes. Immunofluorescence staining of skin sections from three healthy controls showing the expression of various integrin subunits (green) in relation to melanocytes (Melan-A, red). Each panel represents a different integrin subunit: ITGα1, ITGα2, ITGα3, ITGα4, ITGα5, ITGα6, ITGα7, ITGαv, ITGβ1, ITGβ3, and ITGβ4. Insets show magnified views of the boxed regions, highlighting integrin localization in or around melanocytes at the dermal-epidermal junction. Scale bar: 50 μm.

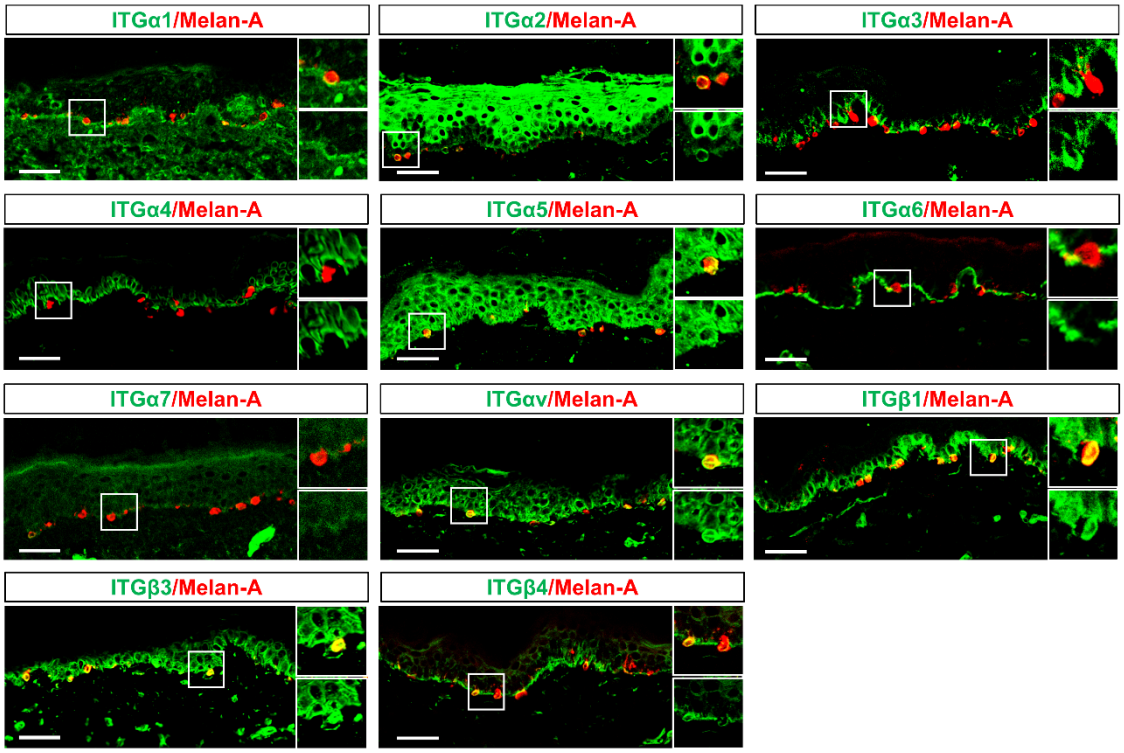

Extended Data Figure 3. Analysis of integrin-laminin interactions in melanocytes from healthy human skin. Proximity ligation assay (PLA) detected protein-protein interactions between integrin subunits and laminin chains in skin sections from three healthy controls. Red signals represent PLA-positive puncta for specific integrin–laminin interactions. Upper panels show positive controls in keratinocytes, for ITGβ4-LNγ2 (a hemidesmosomal component), ITGβ1-LNγ2, ITGβ1-LNα5, and ITGα6-LNα5. Lower panels show PLA signals for integrin–laminin α2 and integrin–laminin γ1 interactions in melanocytes, identified by c-Kit (green). Nuclei are counterstained with 4′,6-diamidino-2-phenylindole (DAPI; blue). Insets show magnified views of boxed areas. Scale bar: 50 μm.

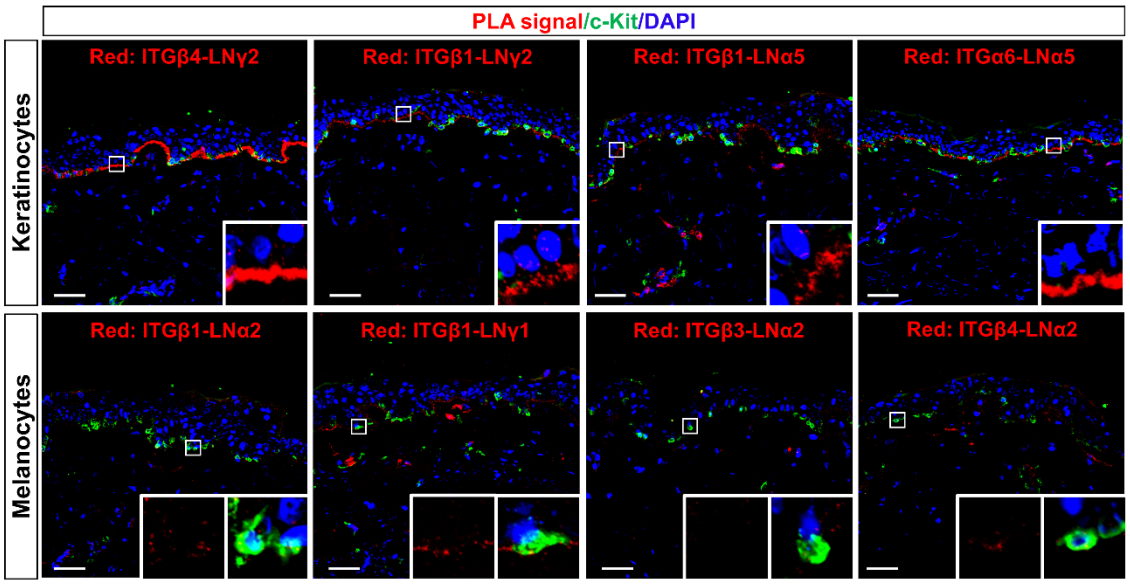

Extended Data Figure 4. Laminin-332 (LN332) induces morphological changes and alters melanogenic protein expression in multiple human melanocyte lines. Representative immunofluorescence images of five melanocyte lines (HEMn-DP, HEMn-MP, LMC, LC1C1022, and M4C0760) cultured on plates coated with either laminin-211 (LN211) or LN332. Cells were stained for Melan-A (red) to assess melanocyte identity and melanogenic status and for phalloidin (blue) to visualize actin cytoskeleton and overall cell morphology following LN332 treatment. Scale bar: 100 µm.

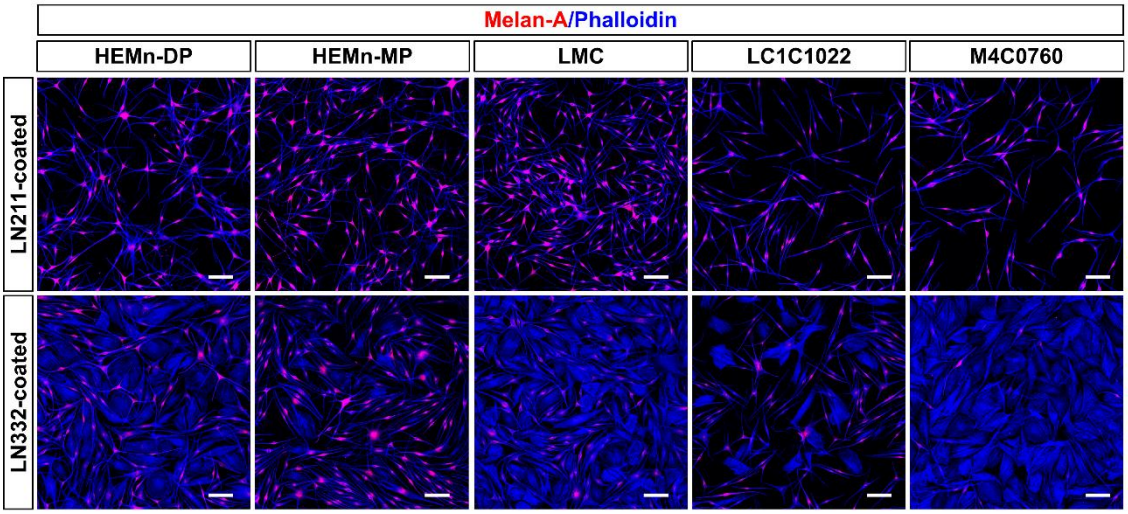

Extended Data Figure 5. Western blot analysis of cytoskeleton components, Hippo pathway, MAPK pathway, and AP-1 family members in laminin-332 (LN332)-induced dedifferentiated melanocytes. **a-d.** Representative immunoblots showing expression levels of proteins related to the cytoskeleton (**a**), Hippo pathway (**b**), MAPK pathway (**c**), and AP-1 family factors (**d**). Lane 1: melanocytes cultured on laminin-211 (LN211; control). Lane 2: melanocytes cultured on LN332. Glyceraldehyde 3-phosphate dehydrogenase (GAPDH) was used as a loading control. **e.** Quantification of protein expression levels relative to GAPDH and normalized to LN211 control. Data are presented as mean ± SEM from three independent experiments.

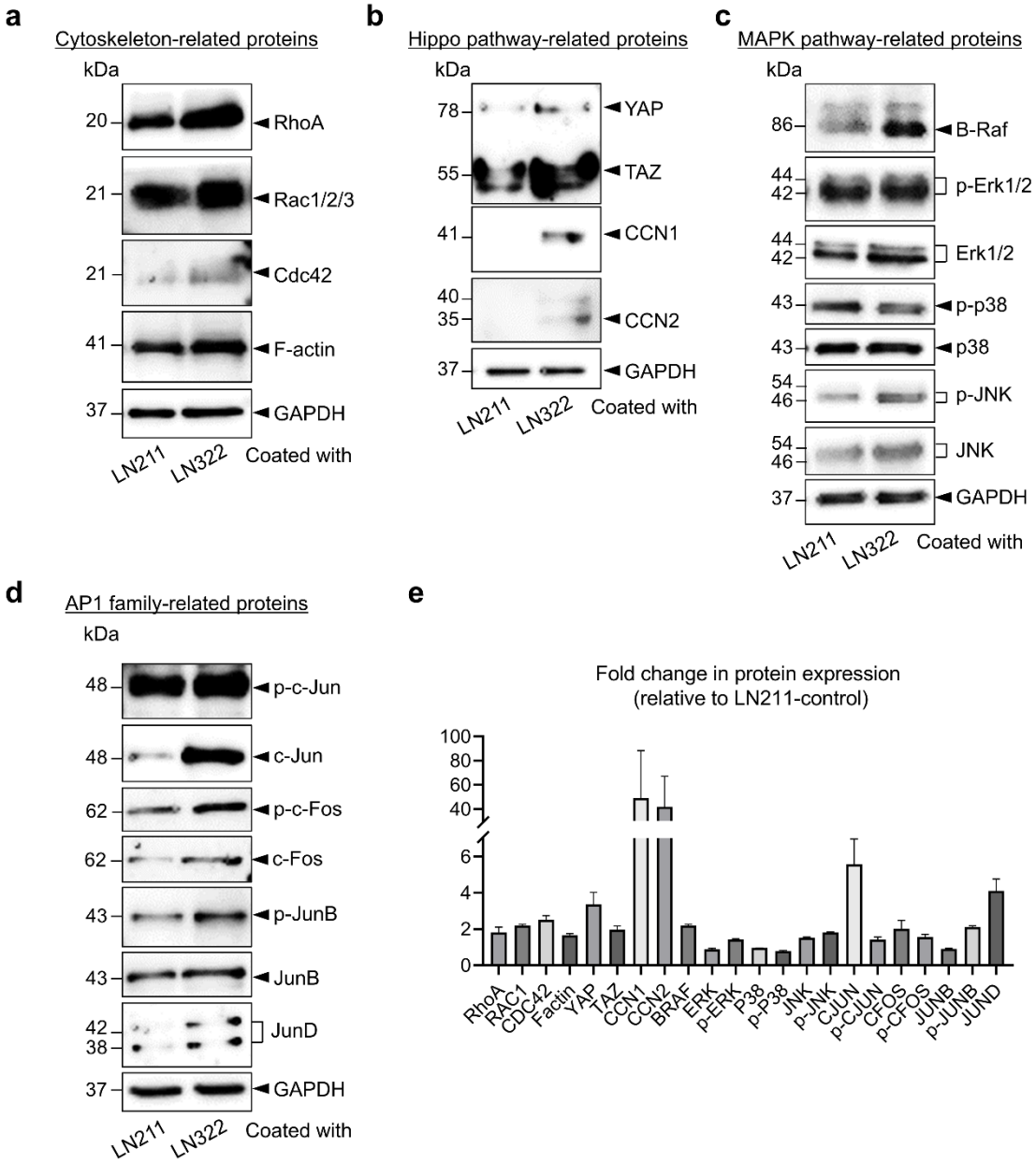
a
Cytoskeleton-related proteins
kDa
20
RhoA
21
Rac1/2/3
21
Cdc42
41
F-actin
37
GAPDH
LN211
LN322
Coated with
b
Hippo pathway-related proteins
kDa
78
YAP
55
TAZ
41
CCN1
40
35
CCN2
37
GAPDH
LN211
LN322
Coated with
c
MAPK pathway-related proteins
kDa
86
B-Raf
44
42
p-Erk1/2
44
42
Erk1/2
43
p-p38
43
p38
54
46
p-JNK
54
46
JNK
37
GAPDH
LN211
LN322
Coated with
d
AP1 family-related proteins
kDa
48
p-c-Jun
48
c-Jun
62
p-c-Fos
62
c-Fos
43
p-JunB
43
JunB
42
38
JunD
37
GAPDH
LN211
LN322
Coated with
e
Fold change in protein expression
(relative to LN211-control)
100
80
60
40
6
4
2
0
RhoA
RAC1
CDC42
Factin
YAP
TAZ
CCN1
CCN2
BRAF
ERK
p-ERK
P38
p-P38
JNK
p-JNK
CJUN
p-CJUN
CFOS
p-CFOS
JUNB
p-JUNB
JUND

Extended Data Figure 6. Influence of vitiligo-associated factors and pharmacological inhibitors on melanocyte dedifferentiation. **a.** Immunofluorescence analysis of Melan-A (red) expression in melanocytes treated with vitiligo-associated stressors, including proinflammatory cytokines (TNFα, IFNβ, IFNγ, IL1β, IL6) and oxidative stress (H_2O_2). Melanocytes were cultured on either noncoated surfaces (left panels) or surfaces coated with laminin-332 (LN332; right panels). Lower panels show enlarged views of selected regions. Scale bar: 100 μm. DAPI, 4′,6-diamidino-2-phenylindole; DMSO, dimethyl sulfoxide. **b.** Effects of JAK inhibitors (ruxolitinib, delgocitinib, baricitinib, abrocitinib, and tofacitinib) on LN332-induced melanocyte dedifferentiation. Melan-A (red) expression was used to assess melanocyte differentiation status. Scale bar: 100 μm. **c.** Effects of tyrosine kinase inhibitors targeting EGFR, EGFR2, IGF-1R, Tie2, c-RET, and ALK on LN332-induced dedifferentiation. Scale bar: 100 μm. **d.** Schematic diagram summarizing the signaling pathways implicated in melanocyte dedifferentiation. ROS, reactive oxygen species.

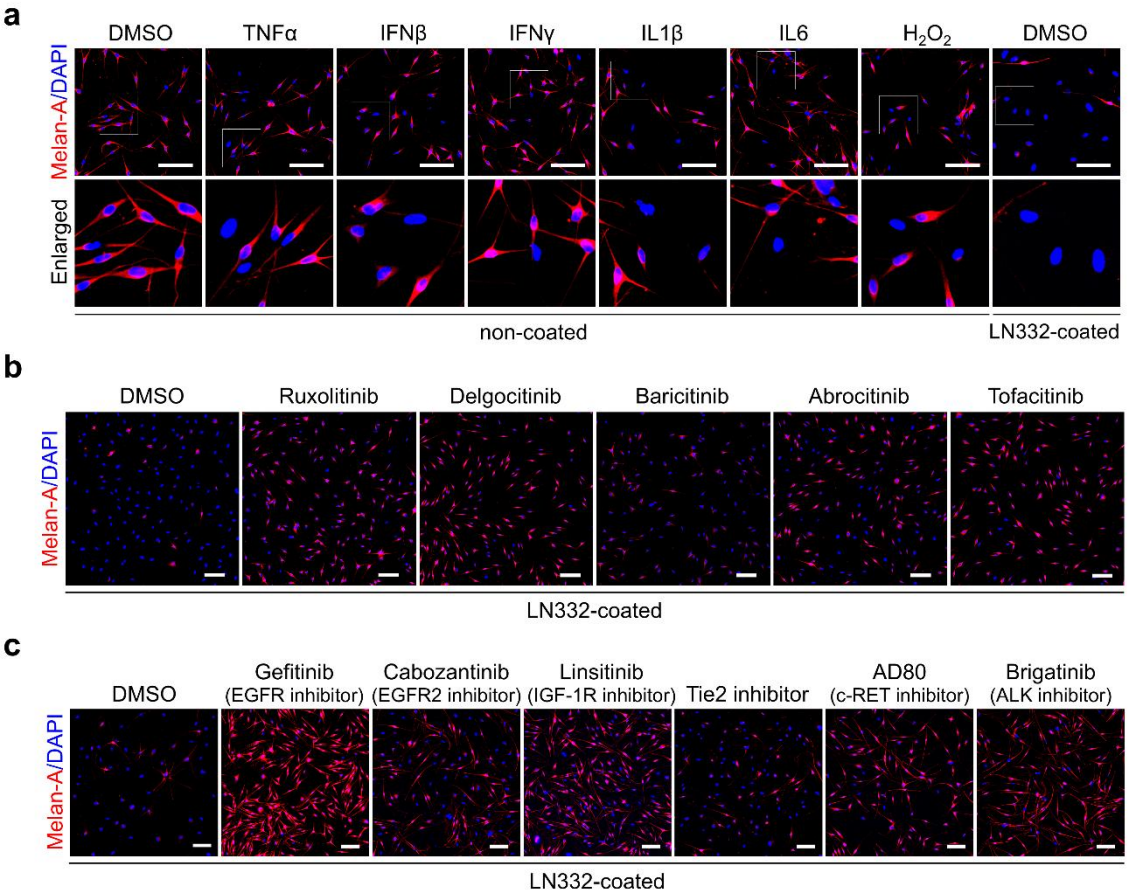
a
DMSO
TNFα
IFNβ
IFNγ
IL1β
IL6
H_2O_2
DMSO
Melan-A/DAPI
Enlarged
non-coated
LN332-coated
b
DMSO
Ruxolitinib
Delgocitinib
Baricitinib
Abrocitinib
Tofacitinib
Melan-A/DAPI
LN332-coated
c
DMSO
Gefitinib (EGFR inhibitor)
Cabozantinib (EGFR2 inhibitor)
Linsitinib (IGF-1R inhibitor)
Tie2 inhibitor
AD80 (c-RET inhibitor)
Brigatinib (ALK inhibitor)
Melan-A/DAPI
LN332-coated

d

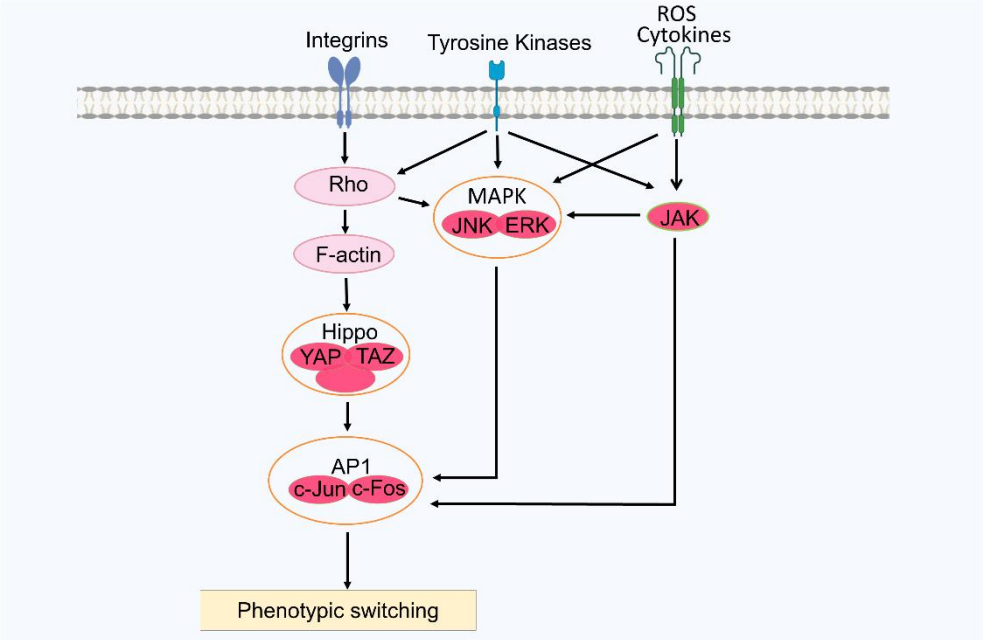
Integrins
Tyrosine Kinases
ROS
Cytokines
Rho
MAPK
JNK
ERK
JAK
F-actin
Hippo
YAP
TAZ
AP1
c-Jun
c-Fos
Phenotypic switching

Extended Data Figure 7. Comparative expression of precursor and melanocyte markers in melanoblasts and melanocytes cultured on laminin-211 (LN211) or laminin-332 (LN332) substrates. Immunofluorescence staining of melanoblasts (top row) and differentiated melanocytes cultured on plates coated with LN211 (middle row) or LN332 (bottom row). Cells were stained for Melan-A, c-Kit, DCT, NGFR, and SOX9 (green) to evaluate the expression of melanocyte lineage and precursor markers. Nuclei were counterstained with 4′,6-diamidino-2-phenylindole (DAPI; blue). Scale bar: 100 μm.

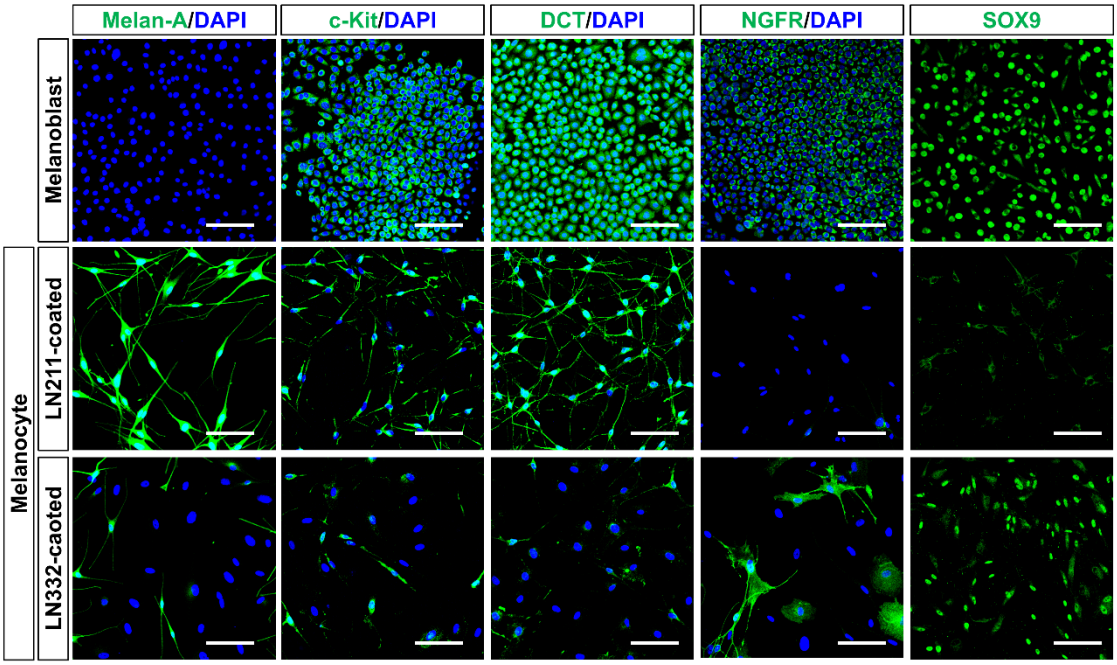

Extended Data Figure 8. Multiparameter immunostaining reveals distinct melanocyte subpopulations following laminin-332 (LN332) treatment. Representative immunofluorescence images of melanocytes cultured on LN332-coated plates and stained with combinations of melanocyte lineage and dedifferentiation markers: **a.** DCT (green), Melan-A (red), and phalloidin (blue); **b.** c-Kit (green), Melan-A (red), and phalloidin (blue); **c.** NGFR (green), Melan-A (red), and phalloidin (blue); **d.** SOX9 (green), Melan-A (red), and phalloidin (blue). Three representative melanocyte states are shown in magnified insets below each panel. #1: Differentiated melanocytes; #2: dedifferentiating melanocytes; #3: dedifferentiated melanocytes. Arrowheads in **c** indicate NGFR/Melan-A double-negative dedifferentiated cells. Arrowheads in **d** indicate SOX9/Melan-A double-negative dedifferentiated cells. Scale bar: 100 μm.

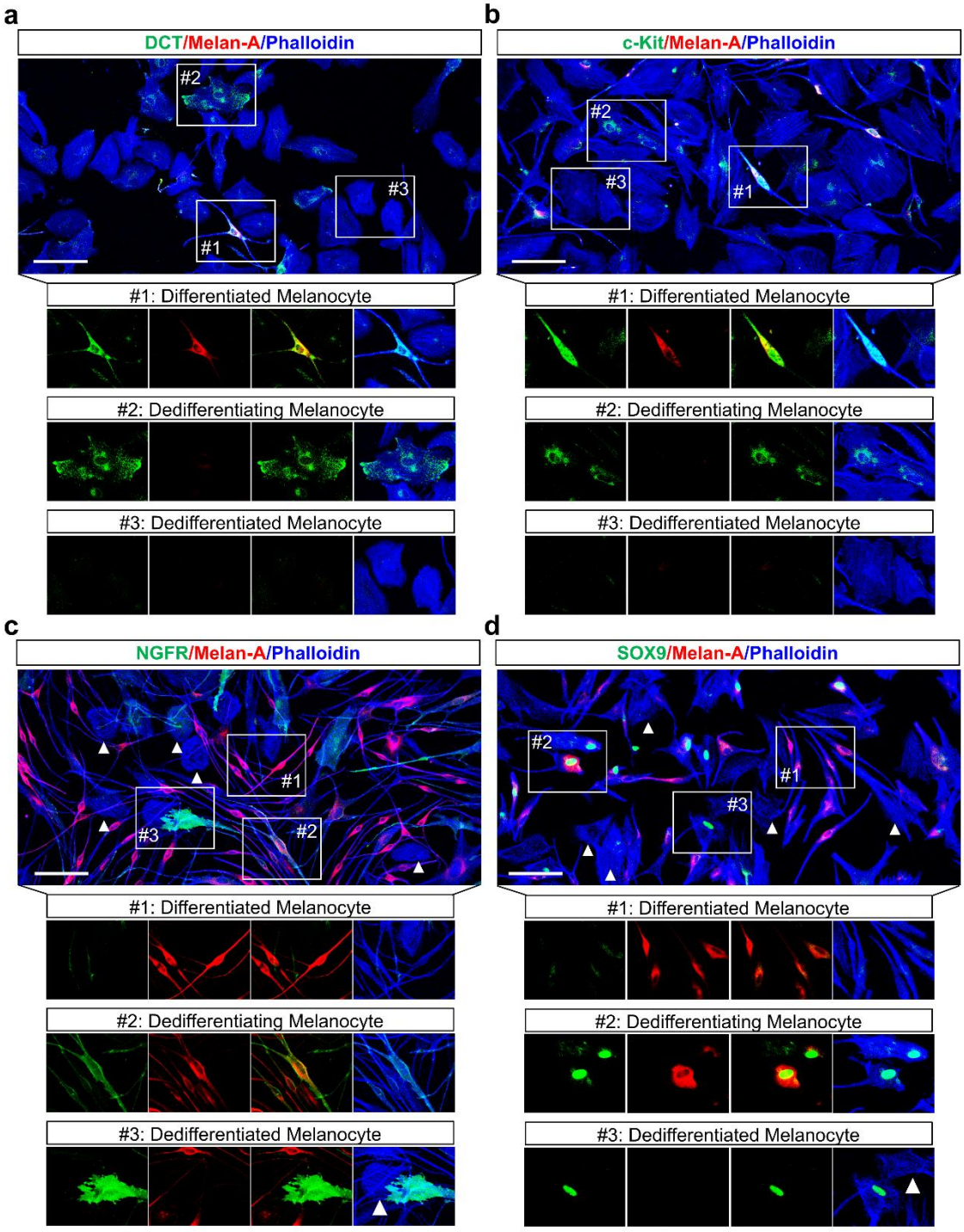
a
DCT/Melan-A/Phalloidin
#2
#3
#1
#1: Differentiated Melanocyte
#2: Dedifferentiating Melanocyte
#3: Dedifferentiated Melanocyte
b
c-Kit/Melan-A/Phalloidin
#2
#3
#1
#1: Differentiated Melanocyte
#2: Dedifferentiating Melanocyte
#3: Dedifferentiated Melanocyte
c
NGFR/Melan-A/Phalloidin
#1
#3
#2
#1: Differentiated Melanocyte
#2: Dedifferentiating Melanocyte
#3: Dedifferentiated Melanocyte
d
SOX9/Melan-A/Phalloidin
#2
#1
#3
#1: Differentiated Melanocyte
#2: Dedifferentiating Melanocyte
#3: Dedifferentiated Melanocyte

Extended Data Figure 9. Identification of dedifferentiating and dedifferentiated melanocytes in vitiligo skin. Immunofluorescence staining of c-Kit (green), NGFR (green), Melan-A (red), and laminin or laminin-332 (LN332; blue) in healthy control and perilesional vitiligo (Vitiligo-PL) skin. Insets highlight melanocytes. Scale bar: 50 µm.

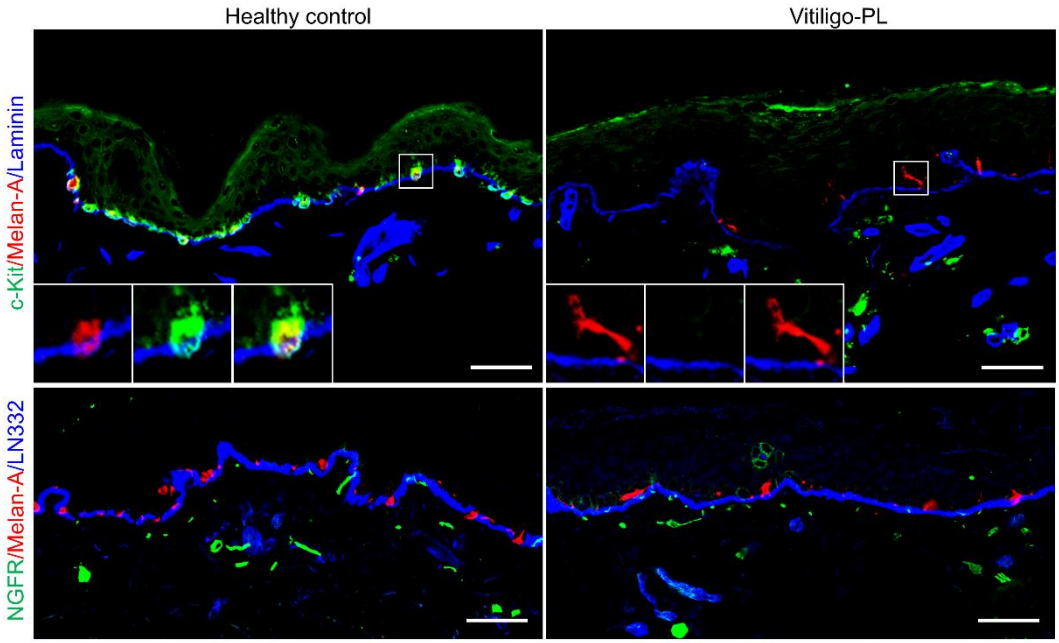

Extended Data Figure 10. Laminin-332 (LN332) reduces mature melanocytes and increases dedifferentiating melanocytes in a three-dimensional (3D) skin model. **a.** Schematic overview of the protocol for constructing a 3D reconstructed human skin model. Keratinocytes and melanocytes were coseeded onto laminin-coated transwell inserts, followed by culture at the air-liquid interface to promote epidermal stratification. **b.** Immunofluorescence staining of TYRP1 (red), DCT (green), and 4′,6-diamidino-2-phenylindole (DAPI; blue) in 3D skin models cultured on substrates coated with laminin-211 (LN211) or LN332. Arrowheads indicate $DCT^{+}/TYRP1^{-}$ melanocytes observed in the LN332-coated model, representing dedifferentiating cells. Scale bar: 50 μm.

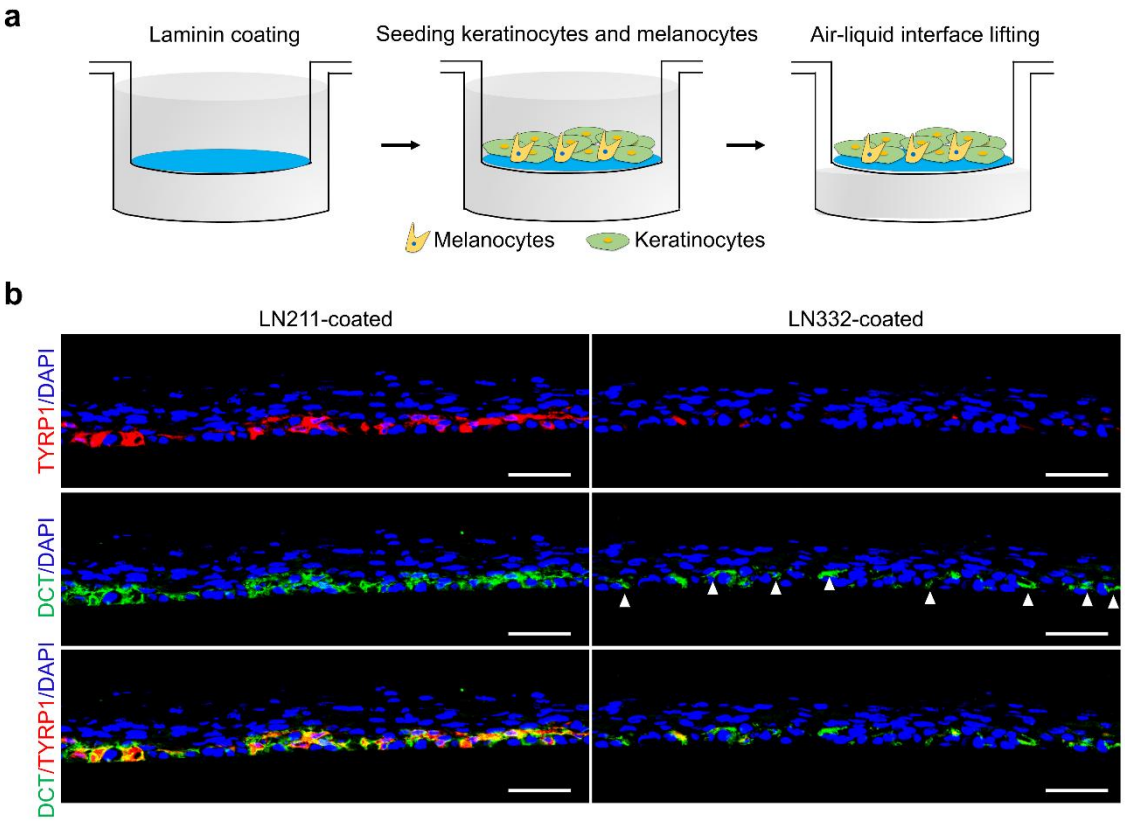

Extended Data Figure 11. Dynamics of melanocyte dedifferentiation in a rhododendrol-induced leukoderma mouse model. **a.** Macroscopic appearance of K14-Kitl mice after topical application of vehicle or rhododendrol. Mice treated with rhododendrol exhibit pronounced hair depigmentation. **b.** Dermoscopic images of dorsal skin from mice treated with vehicle or rhododendrol, showing depigmented patches in rhododendrol-treated skin. **c.** Immunofluorescence staining of TYRP1 (red), DCT (green), c-Kit (green), and laminin (blue) in mouse dorsal skin treated with increasing concentrations of rhododendrol (5%, 10%, 15%). Scale bar: 50 μm. Arrowheads indicate c-Kit^{+}/TYRP1^{-} or DCT^{+}/TYRP1^{-} dedifferentiating melanocytes.

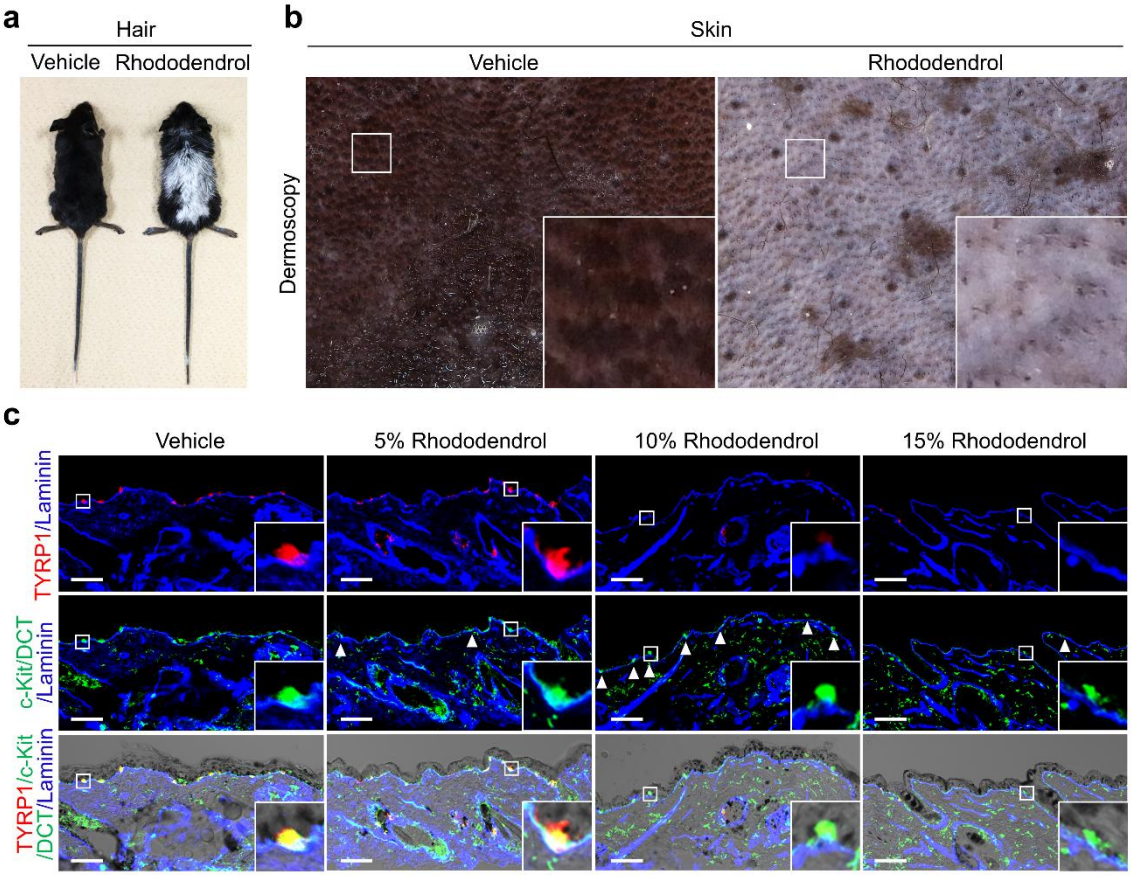

Extended Data Figure 12. SP600125 promotes redifferentiation of melanocytes in *ex vivo*-cultured skin from patients with vitiligo. **a.** Schematic illustration of the *ex vivo* culture system using lesional skin from patients with vitiligo. Skin explants were sectioned and cultured for 1 week in the presence of dimethyl sulfoxide (DMSO; vehicle control) or the JNK inhibitor SP600125. **b.** Immunofluorescence staining of Melan-A (red), DCT (green), and type IV collagen (Col IV, blue) in *ex vivo*-cultured vitiligo skin. Arrowheads indicate DCT^{+}/Melan-A^{-} dedifferentiating melanocytes, which are prevalent in DMSO-treated epidermis. Inset images show higher magnification of boxed regions, illustrating representative dedifferentiated and redifferentiated melanocytes. Scale bar: 50 μm.

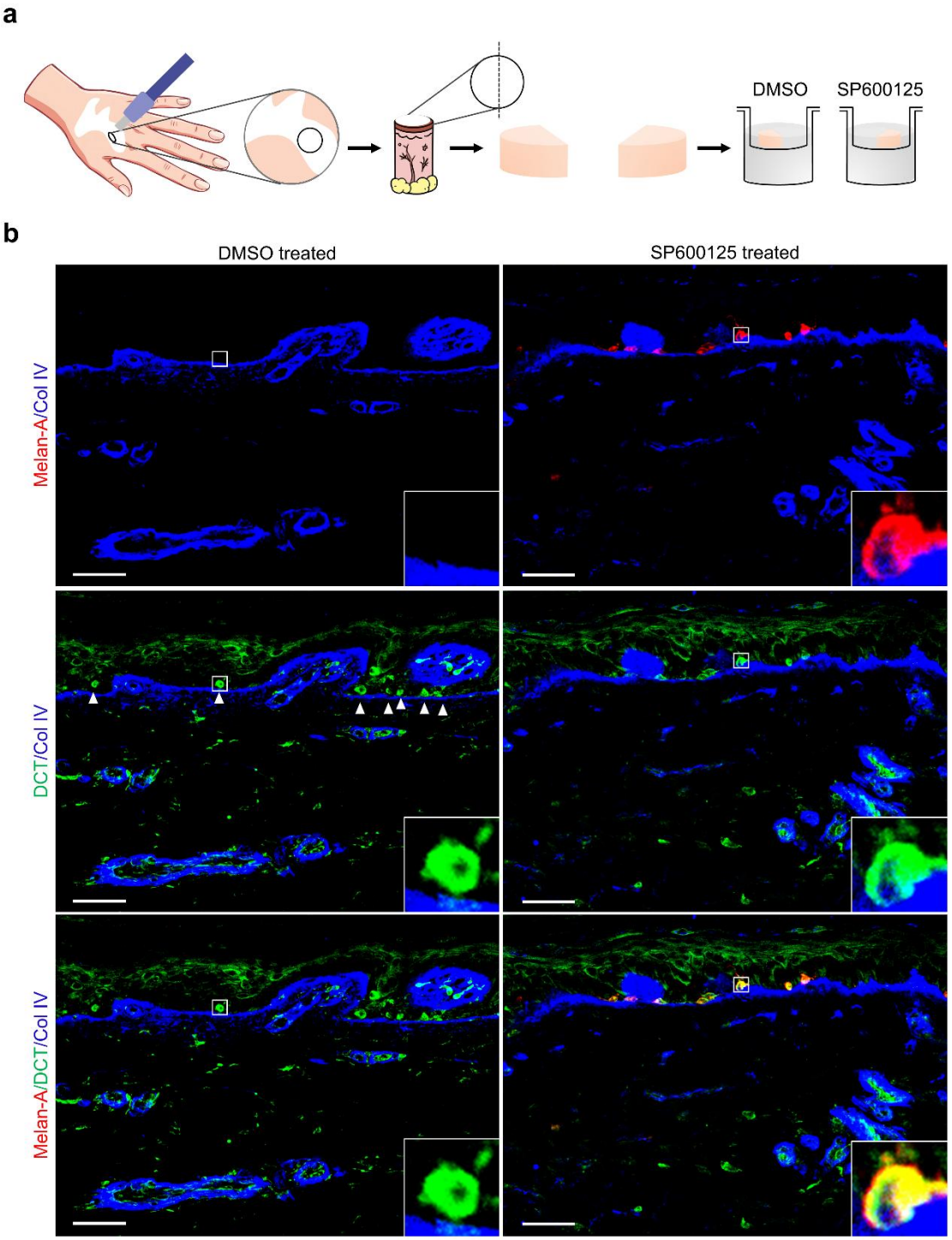
a
DMSO
SP600125
b
DMSO treated
SP600125 treated
Melan-A/Col IV
DCT/Col IV
Melan-A/DCT/Col IV

Extended Data Figure 13. Analysis of membrane-type matrix metalloproteinase (MT-MMP)-mediated laminin-332 (LN332) degradation by melanocytes. **a.** Immunofluorescence staining of MT1-MT6-MMPs (green) and Melan-A (red) in normal human epidermis. Insets show representative melanocytes coexpressing specific MT-MMPs. Scale bar: 50 μm. **b-c.** Quantitative PCR analysis of MT1-MMP (MMP14) (**b**) and MT4-MMP (MMP17) (**c**) mRNA expression across various human cell types. GAPDH, glyceraldehyde 3-phosphate dehydrogenase. **d.** Cell line abbreviations used in **b** and **c**. **e.** LN332 degradation assay using control and MT-MMP-silenced melanocytes. Cells were cultured on LN332-coated plates and stained for laminin (green) and nuclei (4′,6-diamidino-2-phenylindole, DAPI; blue). Scale bar: 100 μm.

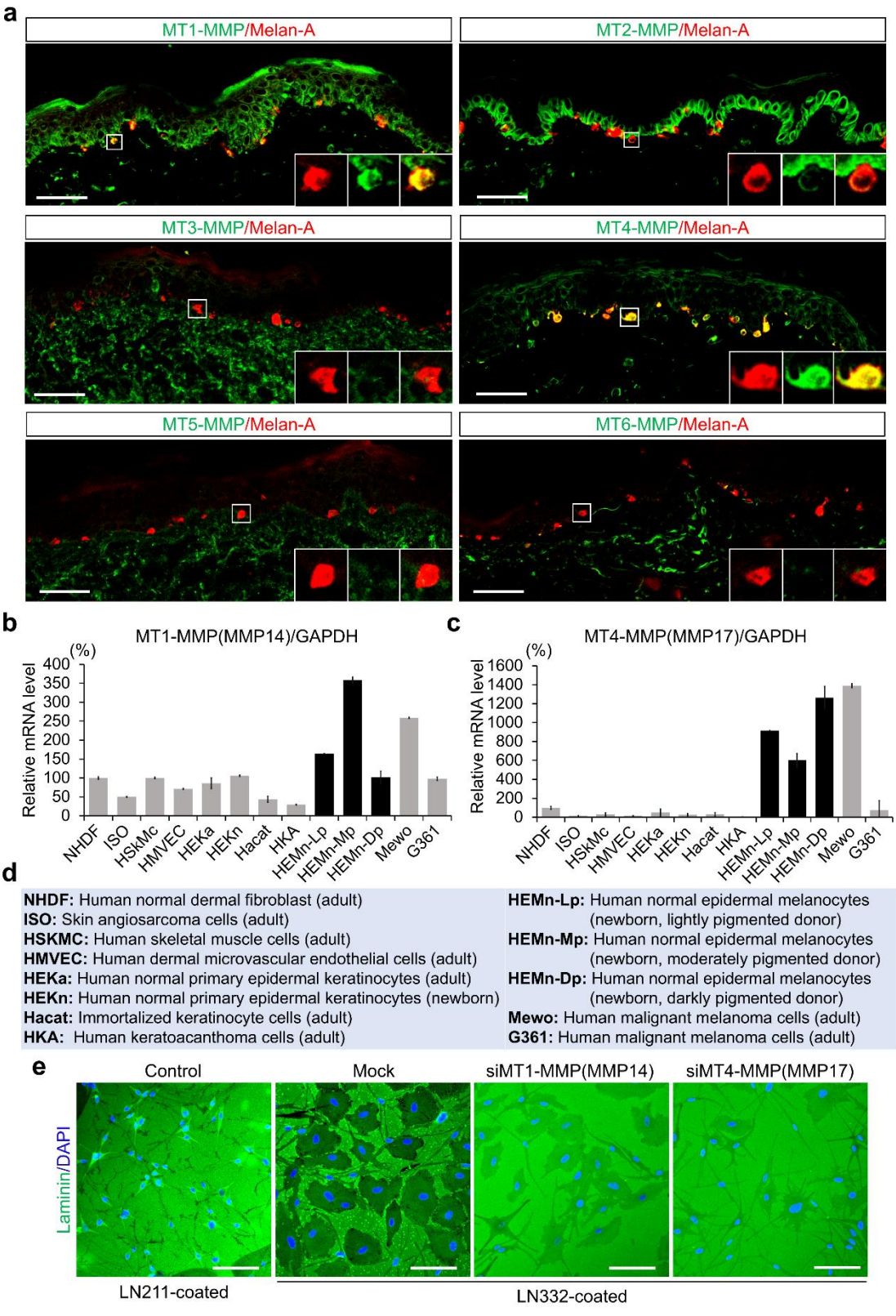
a
MT1-MMP/Melan-A
MT2-MMP/Melan-A
MT3-MMP/Melan-A
MT4-MMP/Melan-A
MT5-MMP/Melan-A
MT6-MMP/Melan-A
b
MT1-MMP(MMP14)/GAPDH
(%)
Relative mRNA level
400
350
300
250
200
150
100
50
0
NHDF
ISO
HSkMc
HMVEC
HEKa
HEKn
Hacat
HKA
HEMn-Lp
HEMn-Mp
HEMn-Dp
Mewo
G361
c
MT4-MMP(MMP17)/GAPDH
(%)
Relative mRNA level
1600
1400
1200
1000
800
600
400
200
0
NHDF
ISO
HSkMc
HMVEC
HEKa
HEKn
Hacat
HKA
HEMn-Lp
HEMn-Mp
HEMn-Dp
Mewo
G361
d
NHDF: Human normal dermal fibroblast (adult)
ISO: Skin angiosarcoma cells (adult)
HSKMC: Human skeletal muscle cells (adult)
HMVEC: Human dermal microvascular endothelial cells (adult)
HEKa: Human normal primary epidermal keratinocytes (adult)
HEKn: Human normal primary epidermal keratinocytes (newborn)
Hacat: Immortalized keratinocyte cells (adult)
HKA: Human keratoacanthoma cells (adult)
HEMn-Lp: Human normal epidermal melanocytes (newborn, lightly pigmented donor)
HEMn-Mp: Human normal epidermal melanocytes (newborn, moderately pigmented donor)
HEMn-Dp: Human normal epidermal melanocytes (newborn, darkly pigmented donor)
Mewo: Human malignant melanoma cells (adult)
G361: Human malignant melanoma cells (adult)
e
Control
Mock
siMT1-MMP(MMP14)
siMT4-MMP(MMP17)
Laminin/DAPI
LN211-coated
LN332-coated

Extended Data Figure 14. Analysis of membrane-type matrix metalloproteinase (MT-MMP) expression in melanocytes from the skin of patients with vitiligo and from mice. **a.** Immunofluorescence staining of MT4-MMP (MMP17), Melan-A, and laminin-332 (LN332) in healthy control and perilesional vitiligo (Vitiligo-PL) human skin. Insets on the right show representative melanocytes (#1-6). Scale bar: 50 μm. **b.** Immunofluorescence staining of MT1-MMP (MMP14), Melan-A, and LN332 in healthy control and Vitiligo-PL human skin. Insets show representative melanocytes. Scale bar: 50 μm. **c.** Immunostaining of MT1-MMP (left) or MT4-MMP (right), Melan-A, and LN332 in K14-Kitl mouse tail skin to assess MT-MMP expression *in vivo*. Scale bar: 50 μm.

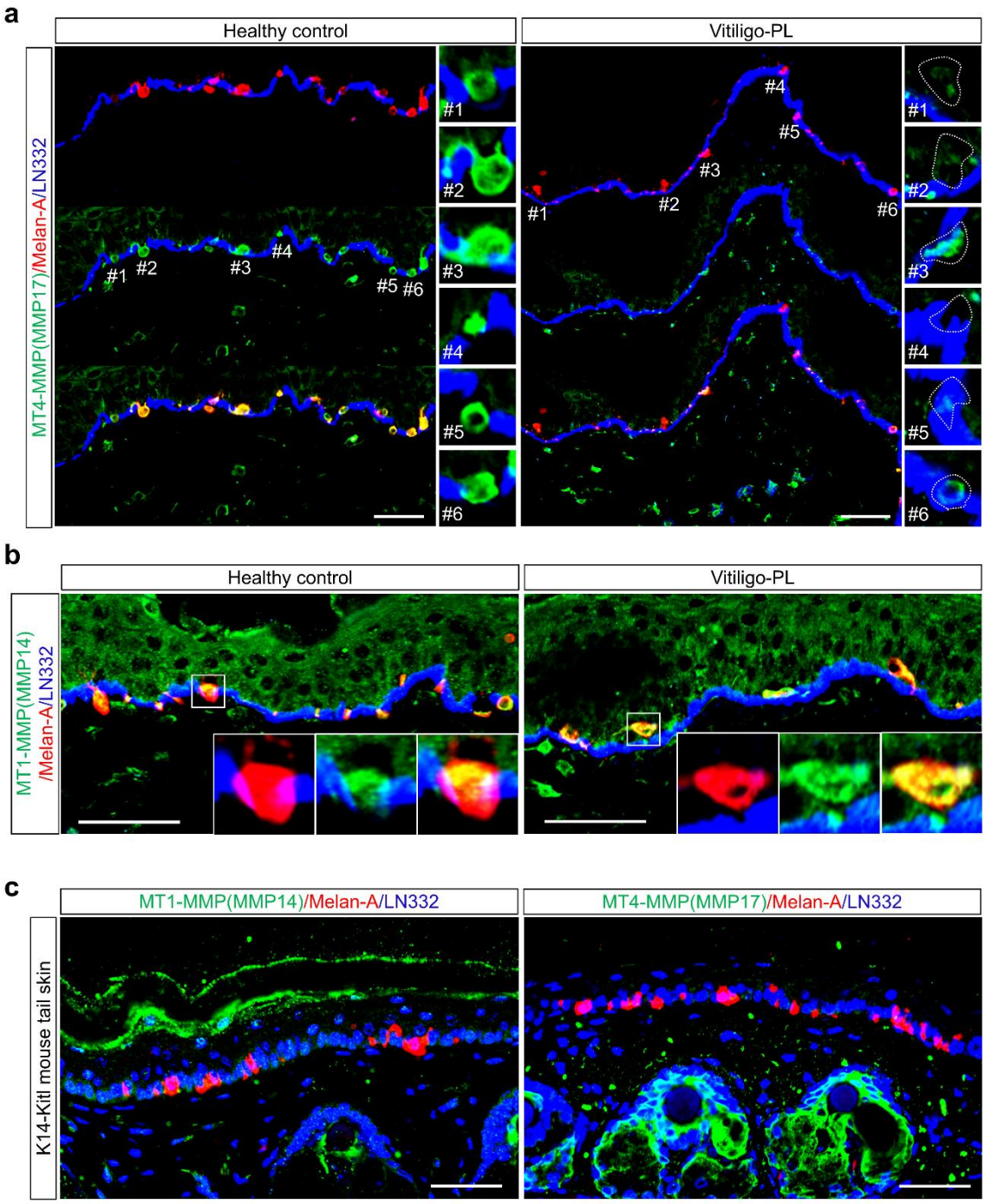
a
Healthy control
Vitiligo-PL
MT4-MMP(MMP17)/Melan-A/LN332
#1
#2
#3
#4
#5
#6
b
Healthy control
Vitiligo-PL
MT1-MMP(MMP14)
/Melan-A/LN332
c
MT1-MMP(MMP14)/Melan-A/LN332
MT4-MMP(MMP17)/Melan-A/LN332
K14-Kitl mouse tail skin

Extended Data Figure 15. Analysis of dystroglycan expression in vitiligo skin and cultured melanocytes. **a.** Immunofluorescence staining of dystroglycan (green), TYRP1 (red), and laminin-332 (LN332; blue) in healthy control and perilesional vitiligo (Vitiligo-PL) skin. Insets enlarge melanocytes. Scale bar: 50 μm. **b.** Expression of dystroglycan in melanocytes cultured on substrates coated with laminin-211 (LN211) or LN332. Immunostaining was performed for dystroglycan (green), Melan-A (red), and phalloidin (blue). Scale bar: 100 μm.

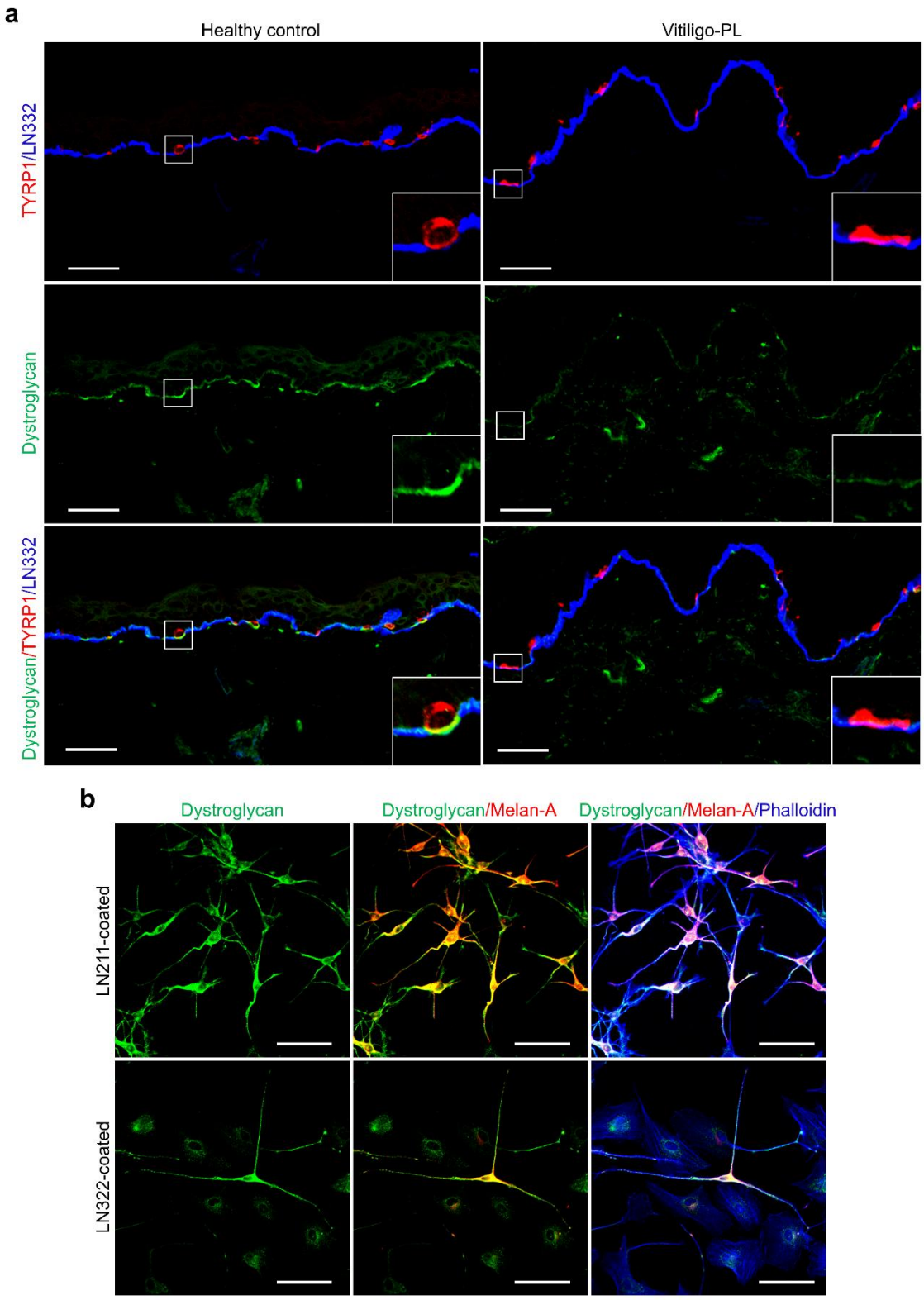
a
Healthy control
Vitiligo-PL
TYRP1/LN332
Dystroglycan
Dystroglycan/TYRP1/LN332
b
Dystroglycan
Dystroglycan/Melan-A
Dystroglycan/Melan-A/Phalloidin
LN211-coated
LN322-coated

Extended Data Figure 16. Schematic illustration of melanocyte dedifferentiation induced by the vitiligo-associated microenvironment. In healthy skin (left), melanocytes adhere to the basement membrane (BM) through dystroglycan-laminin-211 interactions and maintain their differentiated state. MMP17 expression contributes to localized remodeling without disrupting homeostasis. In vitiligo skin (right), increased laminin-332 (LN332) exposure and integrin α3β1 engagement activate intracellular signaling cascades involving F-actin reorganization and the Hippo and MAPK pathways, ultimately converging on c-Jun activation. This signaling switch promotes melanocyte dedifferentiation.

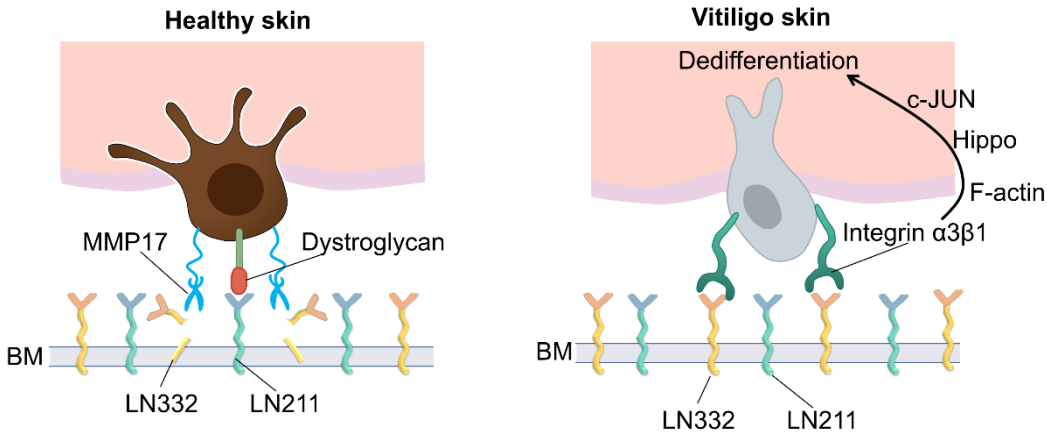

Supplementary Tables

Table S1. Clinical characteristics of the patients

Patient No.	Sex	Age (years)	Type	Biopsy Site	Activity
1[§]	M	72	Nonsegmental vitiligo	Back	Progressive
2[§]	F	49	Nonsegmental vitiligo	Lumbar	Stable
3	M	44	Nonsegmental vitiligo	Back	Progressive
4	F	33	Nonsegmental vitiligo	Axilla	Progressive
5	F	71	Nonsegmental vitiligo	Elbow	Stable
6[§]	F	23	Nonsegmental vitiligo	Abdomen	Stable
7[§]	M	30	Nonsegmental vitiligo	Lateral abdomen	Progressive
8[§]	F	20	Nonsegmental vitiligo	Abdomen	Progressive
9	M	68	Nonsegmental vitiligo	Back	Progressive
10	F	49	Nonsegmental vitiligo	Abdomen	Progressive
11	F	62	Nonsegmental vitiligo	Neck	Stable
12	M	47	Nonsegmental vitiligo	Axilla	Progressive
13[*]	M	76	Nonsegmental vitiligo	Wrist	Progressive
14[*]	F	69	Nonsegmental vitiligo	Back of the hand	Progressive
15	M	47	Nonsegmental vitiligo	Arm	Stable

[§]Samples for electron microscopy.

*Samples for *ex vivo* skin culture.

Abbreviations: F: female; M: male.

Table S2. List of primary antibodies used for immunofluorescence and immunohistochemical analyses

Antibody Name	Host, Isotype, and Subclass	Dilution	Catalog No.	Company Name
Laminin	Rabbit	1:100	ab11575	Abcam
Laminin α1	Mouse IgG1	1:100	AMAb91091	Sigma-Aldrich
Laminin α2	Rat IgG1	1:100	L0663	Sigma-Aldrich
Laminin α3	Mouse IgG2a	1:100	FDV-0024	Funakoshi
Laminin α4	Rabbit	1:100	SAB4501719	Sigma-Aldrich
Laminin α5	Mouse IgG1	1:100	MABT39	Sigma-Aldrich
Laminin β1	Rat IgG1	1:100	ab44941	Abcam
Laminin β2	Mouse IgG1	1:100	AMAb91096	Sigma-Aldrich
Laminin β3	Rabbit	1:100	26795-1-AP	Proteintech
Laminin γ1	Rat IgG2a	1:100	ab80580	Abcam
Laminin γ2	Rabbit	1:100	SAB2700481	Sigma-Aldrich
Laminin-332	Mouse IgG1	1:100	ab78286	Abcam
Integrin α1	Mouse IgG1	1:100	NBP2-76478	Novus Biologicals
Integrin α2	Mouse IgG1	1:100	NBP2-76483	Novus Biologicals
Integrin α3	Mouse IgG2a	1:100	NBP1-97691	Novus Biologicals
Integrin α4	Rabbit	1:100	19676-1-AP	Proteintech
Integrin α5	Rabbit	1:100	27224-1-AP	Proteintech
Integrin α6	Mouse IgG2b	1:100	ab20142	Abcam
Integrin α7	Mouse IgG1	1:100	ab195959	Abcam
Integrin αv	Rabbit	1:100	100563-T08	Sino Biological
Integrin β1	Mouse IgG2a	1:100	ab30388	Abcam
Integrin β1	Rabbit	1:100	PA532887	Thermo Fisher
Integrin β3	Rabbit	1:100	100458-T08	Sino Biological
Integrin β4	Rabbit	1:100	PB9007	Boster Bio
Dystroglycan	Rabbit	1:100	11017-1-AP	Proteintech
DDR	Goat	1:100	AF2396	R&D Systems
Melan-A	Mouse IgG2b	1:100	917901	BioLegend

c-Kit	Goat	1:100	AF332	R&D Systems
c-Kit	Rat IgG2b	1:100	NBP1-43359	Novus Biologicals
PMEL17	Rabbit	1:100	ab137078	Abcam
TYRP1	Mouse IgG2a	1:100	917801	BioLegend
Neurofilament	Rabbit	1:100	2837	Cell Signaling Technology
COL2	Rabbit	1:100	28459-1-AP	BioLegend
α-SMA	Mouse IgG2a	1:100	M0851	Dako
SOX9	Rabbit	1:100	AB5535	Sigma-Aldrich
NGFR	Rabbit	1:100	ab52987	Abcam
DCT	Mouse IgG2a	1:100	sc-74439	Santa Cruz Biotechnology
Collagen IV	Rabbit	1:100	ab19808	Abcam
F-actin	Mouse IgM	1:100	ab205	Abcam
p-JUN	Rabbit	1:100	3270S	Cell Signaling Technology
His-Tag	Rabbit	1:100	12698	Cell Signaling Technology
MT1-MMP	Rabbit	1:100	ARG57921	Arigo Biolaboratories
MT2-MMP	Rabbit	1:100	HPA040390	Sigma-Aldrich
MT3-MMP	Rabbit	1:100	HPA023693	Sigma-Aldrich
MT4-MMP	Rabbit	1:100	PA5-28219	Thermo Fisher
MT5-MMP	Rabbit	1:100	AB924	R&D Systems
MT6-MMP	Mouse IgG1	1:100	MAB11421	R&D Systems
Rabbit IgG Control	Rabbit	1:100	ab172730	Abcam
Mouse IgG Control	Mouse	1:100	ab37355	Abcam
Alexa Fluor 633 Phalloidin		1:500	A22284	Thermo Fisher

Table S3. List of secondary antibodies used for immunofluorescence and immunohistochemical analyses

Antibody Name	Host	Dilution	Catalog No.	Company Name
Alexa Fluor Plus 488 Goat Anti-Rabbit IgG (H+L)	Goat	1:1,000	A32731	Invitrogen
Alexa Fluor Plus 555 Goat Anti-Rabbit IgG (H+L)	Goat	1:1,000	A32732	Invitrogen
Alexa Fluor Plus 647 Goat Anti-Rabbit IgG (H+L)	Goat	1:1,000	A32733	Invitrogen
Alexa Fluor Plus 488 Goat Anti-Mouse IgG (H+L)	Goat	1:1,000	A32723	Invitrogen
Alexa Fluor Plus 555 Goat Anti-Mouse IgG (H+L)	Goat	1:1,000	A32727	Invitrogen
Alexa Fluor Plus 647 Goat Anti-Mouse IgG (H+L)	Goat	1:1,000	A21236	Invitrogen
Goat Anti-Mouse IgG1, Alexa Fluor 488	Goat	1:1,000	A21121	Invitrogen
Goat Anti-Mouse IgG1, Alexa Fluor 555	Goat	1:1,000	A21127	Invitrogen
Goat Anti-Mouse IgG1, Alexa Fluor 647	Goat	1:1,000	A21240	Invitrogen
Goat Anti-Mouse IgG2a, Alexa Fluor 488	Goat	1:1,000	A21131	Invitrogen
Goat Anti-Mouse IgG2a, Alexa Fluor 555	Goat	1:1,000	A21137	Invitrogen
Goat Anti-Mouse IgG2a, Alexa Fluor 647	Goat	1:1,000	A21136	Invitrogen
Goat Anti-Mouse IgG2b, Alexa Fluor 488	Goat	1:1,000	A21141	Invitrogen
Goat Anti-Mouse IgG2b, Alexa Fluor 555	Goat	1:1,000	A21147	Invitrogen
Goat Anti-Mouse IgG2b, Alexa Fluor 647	Goat	1:1,000	A21242	Invitrogen
Goat Anti-Rat IgG (H+L), Alexa Fluor 488	Goat	1:1,000	A11006	Invitrogen
Goat Anti-Rat IgG (H+L), Alexa Fluor 555	Goat	1:1,000	A48263	Invitrogen
Goat Anti-Rat IgG (H+L), Alexa Fluor 647	Goat	1:1,000	A21247	Invitrogen
Donkey Anti-Goat IgG (H+L), Alexa Fluor Plus 488	Donkey	1:1,000	A32814	Invitrogen
Donkey Anti-Rabbit IgG (H+L), Alexa Fluor Plus 555	Donkey	1:1,000	A32794	Invitrogen
Donkey Anti-Mouse IgG (H+L), Alexa Fluor Plus 647	Donkey	1:1,000	A32787	Invitrogen

Table S4. List of primary antibodies used for Western blot analyses

Antibody Name	Host, Isotype, and Subclass	Dilution	Catalog No.	Company Name
c-Kit	Rabbit	1:1,000	3074	Cell Signaling Technology
TYR	Mouse IgG2a	1:1,000	SC20035	Santa Cruz Biotechnology
Melan-A	Rabbit	1:100	ab51061	Abcam
TYRP1	Mouse IgG2a	1:100	sc58438	Santa Cruz Biotechnology
PMEL17	Mouse IgG1	1:100	sc377325	Santa Cruz Biotechnology
DCT	Mouse IgG2a	1:100	sc74439	Santa Cruz Biotechnology
RhoA	Rabbit	1:1,000	2117	Cell Signaling Technology
RAC1/2/3	Rabbit	1:1,000	2465	Cell Signaling Technology
CDC42	Rabbit	1:1,000	2462	Cell Signaling Technology
F-actin	Mouse IgM	1:100	ab205	Abcam
YAP	Rabbit	1:1,000	8418	Cell Signaling Technology
CCN1	Rabbit	1:1,000	14479	Cell Signaling Technology
CCN2	Rabbit	1:1,000	86641	Cell Signaling Technology
BRAF	Rabbit	1:1,000	9433	Cell Signaling Technology
Erk	Rabbit	1:1,000	4695	Cell Signaling Technology
p-Erk	Rabbit	1:1,000	4370	Cell Signaling Technology
p38	Rabbit	1:1,000	8690	Cell Signaling Technology
p-p38	Rabbit	1:1,000	4511	Cell Signaling Technology
JNK	Rabbit	1:1,000	9252	Cell Signaling Technology
p-JNK	Rabbit	1:1,000	4668	Cell Signaling Technology
c-Jun	Rabbit	1:1,000	9165	Cell Signaling Technology
p-c-Jun	Rabbit	1:1,000	3270	Cell Signaling Technology
c-Fos	Rabbit	1:1,000	4384	Cell Signaling Technology
p-c-Fos	Rabbit	1:1,000	5348	Cell Signaling Technology
JunB	Rabbit	1:1,000	3753	Cell Signaling Technology
p-JunB	Rabbit	1:1,000	8053	Cell Signaling Technology
JunD	Rabbit	1:1,000	5000	Cell Signaling Technology
GAPDH	Rabbit	1:1,000	52118	Cell Signaling Technology

Table S5. List of siRNAs used for siRNA-mediated knockdown in melanocytes

SiRNA Name	Species	Assay ID	Catalog No.	Company Name
Dystroglycan Silencer Select	Human	s3908	4394420	Thermo Fisher Scientific
LARGE Silencer Select	Human	s17620	4392420	Thermo Fisher Scientific
Integrin α1 Silencer Select	Human	s7532	4390824	Thermo Fisher Scientific
Integrin α3 Silencer Select	Human	s7543	4390824	Thermo Fisher Scientific
Integrin α4 Silencer Select	Human	s7545	4390824	Thermo Fisher Scientific
Integrin α6 Silencer Select	Human	s7493	4390824	Thermo Fisher Scientific
Integrin αv Silencer Select	Human	s7570	4390824	Thermo Fisher Scientific
Integrin β1 Silencer Select	Human	s7576	4390824	Thermo Fisher Scientific
Integrin β3 Silencer Select	Human	s7581	4392420	Thermo Fisher Scientific
YAP1 Silencer Select	Human	s20366	4392420	Thermo Fisher Scientific
TEAD1 Silencer	Human	116315	AM16708	Thermo Fisher Scientific
CCN1 Silencer Select	Human	s7244	4390824	Thermo Fisher Scientific
CCN2 Silencer Select	Human	s3708	4390824	Thermo Fisher Scientific
BRAF Silencer Select	Human	s2081	4392420	Thermo Fisher Scientific
ERK1 Silencer Select	Human	s11137	4390824	Thermo Fisher Scientific
JNK1 Silencer Select	Human	s11152	4392420	Thermo Fisher Scientific
JUN Silencer Select	Human	s7659	4392420	Thermo Fisher Scientific
CFOS Silencer Select	Human	s5340	4392420	Thermo Fisher Scientific
PIK3CA Silencer Select	Human	s10522	4392420	Thermo Fisher Scientific
GSK3B Silencer Select	Human	s6239	4390824	Thermo Fisher Scientific
CTNNB1 Silencer Select	Human	s436	4390824	Thermo Fisher Scientific
NOTCH1 Silencer Select	Human	s453558	4392420	Thermo Fisher Scientific
SOX9 Silencer Select	Human	s13306	4392420	Thermo Fisher Scientific
MT1-MMP Silencer	Human	104074	AM51331	Thermo Fisher Scientific
MT4-MMP Silencer	Human	23831	AM16708	Thermo Fisher Scientific

Table S6. List of compounds used for *in vitro* drug treatments

Compound Category	Compound Name	Treatment Concentration	Catalog No.	Company Name
Actin inhibitors	Cytochalasin D	1 μM	034-25881	FUJIFILM Wako Pure Chemical Corporation
	Latrunculin B	250 nM	AG-CN2-0031-M001	AdipoGen Life Sciences
	Chaetoglobosin A	500 nM	BVT-0092-M001	AdipoGen Life Sciences
Actin activator	Jasplakinolide	5 nM	AG-CN2-0037-C100	AdipoGen Life Sciences
Rho/Rac/Cdc42 activator	Rho/Rac/Cdc42 Activator I	2 μg/ml	CN04A	Cytoskeleton, Inc.
ROCK activator	Narciclasine	40 nM	SML2805	Sigma-Aldrich
YAP inhibitors	TED-347	150 nM	HY-125269	MedchemExpress
	Verteporfin	300 nM	HY-B0146	MedchemExpress
YAP activators	PY-60	10 μM	HY-141644	MedchemExpress
	GA-017	10 μM	HY-147082	MedchemExpress
JNK inhibitors	SP600125	50 μM	HY-12041	MedchemExpress
	T-5224	25 μM	HY-12270	MedchemExpress
JNK activator	Anisomycin	100 nM	HY-18982	MedchemExpress

Table S7. List of compounds used for *in vivo* drug treatments

Compound Category	Compound Name	Treatment Concentration	Catalog No.	Company Name
Actin inhibitor	Chaetoglobosin A	500 μM	BVT-0092-M001	AdipoGen Life Sciences
Actin activator	Jasplakinolide	10 μM	AG-CN2-0037-C100	AdipoGen Life Sciences
YAP inhibitor	Verteporfin	500 μM	HY-B0146	MedchemExpress

YAP activator	PY-60	500 μM	HY-141644	MedchemExpress
JNK inhibitors	SP600125	500 μM	HY-12041	MedchemExpress
JNK activator	Anisomycin	200 μM	HY-18982	MedchemExpress

Table S8. List of compounds used for *ex vivo* drug treatments

Compound Category	**Compound Name**	**Treatment Concentration**	**Catalog No.**	**Company Name**
Actin inhibitor	Latrunculin B	2 μM	AG-CN2-0031-M001	AdipoGen Life Sciences
	Chaetoglobosin A	7.5 μM	BVT-0092-M001	AdipoGen Life Sciences
Actin activator	Jasplakinolide	50 nM	AG-CN2-0037-C100	AdipoGen Life Sciences
YAP inhibitor	TED-347	1 μM	HY-125269	MedchemExpress
	Verteporfin	1 μM	HY-B0146	MedchemExpress
YAP activator	PY-60	10 μM	HY-141644	MedchemExpress
	GA-017	10 μM	HY-147082	MedchemExpress
JNK inhibitors	SP600125	50 μM	HY-12041	MedchemExpress
	T-5224	25 μM	HY-12270	MedchemExpress
JNK activator	Anisomycin	500 nM	HY-18982	MedchemExpress